A multifidelity quantile-based approach for confidence sets of random excursion sets with application to ice-sheet dynamics*

Kevin Bulthuis[†‡], Frank Pattyn[‡], and Maarten Arnst[†]

Abstract. In this paper, we address uncertainty quantification of physics-based computational models when the quantity of interest concerns geometrical characteristics of their spatial response. Within the probabilistic context of the random set theory, we develop the concept of confidence sets that either contain or are contained within an excursion set of the spatial response with a specified probability level. We seek such confidence sets in a parametric family of nested candidate sets defined as a parametric family of sublevel or superlevel sets of a membership function. We show that the problem of identifying a confidence set with a given probability level in such a parametric family is equivalent to a problem of estimating a quantile of a random variable obtained as a global extremum of the membership function over the complement of the excursion set. To construct such confidence sets, we propose a computationally efficient bifidelity method that exploits a spectral representation of this random variable to reduce the required number of evaluations of the computational model. We show the interest of this concept of confidence sets and the efficiency gain of the proposed bifidelity method in an illustration relevant to the retreat of the grounded portion of the Antarctic ice sheet.

Key words. excursion sets, confidence sets, quantile estimation, stochastic computational models, ice-sheet projections

AMS subject classifications. 68Q25, 68R10, 68U05

1. Introduction.

There are many applications in which interest is directed towards determining within a spatial domain a subregion where the spatial response of a (physics-based) computational model exceeds a specified threshold. This task may serve to determine, for instance, a critical level of safety or help distinguish between different characteristics of the spatial response. Examples include applications in chemical contamination, geophysics (volcanic hazards [6]) and climatology (heat-wave detection [12]). In practice, computational models of such complex systems may have many physical parameters that may be uncertain due to data limitations and modeling hypotheses. Hence, understanding and quantifying the impact of the input uncertainties on geometrical characteristics of the spatial response of a computational model is an interesting problem in uncertainty quantification.

Here, we seek to quantify uncertainty in excursion sets of spatial responses of computational models using the concept of confidence sets that either contain an excursion set of the spatial response or are contained within an excursion set of the spatial response with a specified confidence level. Such confidence sets were first introduced in [7, 13, 14, 15] in a context of Bayesian inference under a stationary Gaussian spatial process prior and further extended to non-stationary and non-Gaussian spatial processes in [27]. From a theoretical

*Submitted to the editors DATE.

Funding: K. Bulthuis would like to acknowledge the Fonds de la Recherche Scientifique de Belgique (F.R.S.-FNRS) for its financial support (F.R.S.-FNRS Research Fellowship).

[†]Aérospatiale et Mécanique, Université de Liège, Liège, Belgium (kevin.bulthuis@uliege.be, maarten.arnst@uliege.be).

[‡]Laboratoire de Glaciologie, Université Libre de Bruxelles, Brussels, Belgium (fpattyn@ulb.ac.be).

point of view, excursion sets of random fields can be studied by using the random set theory [4, 5, 21] or the geometry theory of random fields [1, 2]. In [4, 7, 13, 14], confidence sets are computed by seeking the optimal confidence set in a parametric family of nested candidate sets by solving either an optimization problem or an equivalent problem of quantile estimation. These references have addressed the numerical solution of these optimization and quantile estimation problems in specific contexts in which the random field is obtained by Bayesian inference under a Gaussian spatial process prior, including kriging methods. In such contexts, the random field can be evaluated everywhere in the spatial domain by using the Gaussian-process or kriging interpolants, and numerous samples of the random field can be simulated at low computational cost.

In this paper, we address the computation of confidence sets of excursion sets of random fields obtained as solution quantities of stochastic computational models with a high computational cost. In this context, the definition and computation of excursion sets and confidence sets must be based on the spatial discretization of the computational model obtained, for instance, with a finite-difference or a finite-element discretization scheme. Based on the random set theory, we propose a spatial discretization of excursion sets and confidence sets that relies on a partitioning of the domain into subsets and testing the exceedance constraints in representative points in these subsets. Such a spatial discretization is shown to have an impact on the stochastic dimension of the problem and the accuracy one may achieve in computing confidence sets.

The computation of confidence sets for computational models with a high computational cost requires computationally efficient methods for the discretization of the stochastic dimension. Monte Carlo methods may lead to a slow decrease of the estimation error as a function of the number of samples, which may be intractable for computational models with a high computational cost or high confidence levels. The use of surrogate models, such as stochastic expansions, may reduce the computational cost but may lead to an additional approximation error. Here, we propose a bifidelity method [17, 19, 29] in which a surrogate model is used further away from the quantile to be estimated and the computational model is used closer to the quantile to be estimated.

As an illustration, we consider a problem of assessing the retreat of the grounded portion of the Antarctic ice sheet (AIS) in response to climate forcing. In this illustration, the grounded portion of the AIS is obtained as an excursion set of a solution quantity of a computational ice-sheet model. We illustrate how the proposed bifidelity method may help reduce the computational cost of computing confidence sets and we show how confidence sets may help to assess with quantified uncertainty the vulnerability of the AIS to climate change.

The paper is organized as follows. In sect. 3, we review the concepts of excursion sets, contour sets, and confidence sets of a random field based on the random set theory [21], and we discuss the identification of an optimal confidence set in a parametric family of nested candidate sets. Then, sect. 4 addresses the spatial discretization, sect. 5 is concerned with the discretization of the stochastic dimension, and sect. 6 provides the illustration.

2. Notations.

We denote a deterministic set by a Latin or a Greek upper case letter such as D or Ω, a random set by a calligraphic upper case letter such as $\mathcal{E}$, and a family of subsets of a topological space or a σ-algebra by a Fraktur upper case letter such as $\mathfrak{F}$. Throughout

this paper, we denote by D a compact subset of the d-dimensional Euclidean space $\mathbb{R}^d$. We use the symbol $\subset$ to denote the strict and non-strict inclusion relations. For a subset $E \subset D$, we denote by E^{c}, $\mathrm{cl}(E)$, $\mathrm{int}(E)$, and $|E|$ the complement in D, the closure, the interior, and the Lebesgue measure of E, respectively. Finally, we denote by $\mathfrak{F}$ the family of all closed subsets of D and by $\mathfrak{L}$ the family of all open subsets of D.

3. Confidence sets for excursion and contour sets.

Let $\{Y(\boldsymbol{x}), \boldsymbol{x} \in D\}$ be a random field defined on a complete probability space $(\Theta, \mathfrak{B}, \mathbb{P})$, indexed by D, with values in $\mathbb{R}$, and with continuous sample paths almost surely.

3.1. Excursion sets, contour sets, and confidence sets.

The positive and negative excursion sets of $\{Y(\boldsymbol{x}), \boldsymbol{x} \in D\}$ for the threshold u are defined by

$$\mathcal{E}_u^+ = \{\boldsymbol{x} \in D : Y(\boldsymbol{x}) \geq u\}, \tag{3.1}$$

$$\mathcal{E}_u^- = \{\boldsymbol{x} \in D : Y(\boldsymbol{x}) \leq u\}. \tag{3.2}$$

Similarly, the contour set of $\{Y(\boldsymbol{x}), \boldsymbol{x} \in D\}$ for the threshold u is defined by

$$\mathcal{E}_u^0 = \{\boldsymbol{x} \in D : Y(\boldsymbol{x}) = u\}. \tag{3.3}$$

Because $\{Y(\boldsymbol{x}), \boldsymbol{x} \in D\}$ has continuous sample paths almost surely, $\mathcal{E}_u^+$, $\mathcal{E}_u^-$, and $\mathcal{E}_u^0$ are closed subsets of D almost surely.

The random set theory, see, for instance, [21], provides a rigorous framework for the definition and description of such excursion and contour sets as set-valued random variables, which requires to be more specific about measurability. Within the random set theory, $\mathcal{E}_u^+$, $\mathcal{E}_u^-$, and $\mathcal{E}_u^0$ are defined as measurable mappings from $(\Theta, \mathfrak{B}, \mathbb{P})$ into $(\mathfrak{F}, \mathfrak{S}(\mathfrak{F}))$, with $\mathfrak{S}(\mathfrak{F})$ the σ-algebra generated by the sets $\{K \in \mathfrak{F} : K \cap F \neq \emptyset\}$ for F running through the family $\mathfrak{F}$ of closed subsets of D. The random set theory provides several descriptors for random closed sets, such as the containment and inclusion functionals, the coverage function, and Vorob'ev quantiles, which are described next. The containment functional of $\mathcal{E}_u^+$ is defined by

$$C_{\mathcal{E}_u^+} : \mathfrak{F} \to [0,1]; F \mapsto C_{\mathcal{E}_u^+}(F) = \mathbb{P}(\mathcal{E}_u^+ \subset F), \tag{3.4}$$

and the inclusion functional of $\mathcal{E}_u^+$ is defined by

$$I_{\mathcal{E}_u^+} : \mathfrak{F} \to [0,1]; F \mapsto I_{\mathcal{E}_u^+}(F) = \mathbb{P}(F \subset \mathcal{E}_u^+). \tag{3.5}$$

Containment and inclusion functionals can be defined similarly for $\mathcal{E}_u^-$. Although, the containment functional may be defined similarly for $\mathcal{E}_u^0$, the definition of the inclusion functional is less meaningful for $\mathcal{E}_u^0$ because $\mathcal{E}_u^0$ is generally of lower dimension than D and its inclusion functional vanishes for all F in $\mathfrak{F}$ of the same dimension as D. Please note that neither the containment functional nor the inclusion functional is a probability measure, except for the case of random singletons. The containment functional (and the inclusion functional for random closed sets that coincide with the closure of their interior almost surely) uniquely determines the probability distribution of a random closed set. The random set theory also

defines further functionals that provide insight into the probability distribution of the random closed set. By limiting $F = \{\boldsymbol{x}\}$ to be a singleton, the inclusion functional

$$I_{\mathcal{E}_u^+}(F) = \mathbb{P}(\boldsymbol{x} \in \mathcal{E}_u^+) = \mathbb{P}(Y(\boldsymbol{x}) \geq u) \equiv p_{\mathcal{E}_u^+}(\boldsymbol{x}) \tag{3.6}$$

reduces to the so-called (one-point) coverage function of $\mathcal{E}_u^+$, which provides the pointwise (marginal) probability of exceeding the threshold u. As a generalization of quantiles of scalar-valued random variables, the random set theory defines the so-called Vorob'ev ρ-quantile

$$Q_\rho^{\mathrm{V}} = \left\{\boldsymbol{x} \in D : p_{\mathcal{E}_u^+}(\boldsymbol{x}) \geq \rho\right\} \tag{3.7}$$

as the superlevel set of the coverage function for the level ρ. Thus, the Vorob'ev ρ-quantile is the set of locations where the pointwise (marginal) probability of exceeding the threshold u is at least ρ. The Vorob'ev quantiles are used in the random set theory to define a notion of expectation for random closed sets [4, 5, 21]; the so-called Vorob'ev expectation is the Vorob'ev quantile whose Lebesgue measure is equal or closest to the expected Lebesgue measure of the random closed set. The Vorob'ev quantiles are also minimizers of the expected distance in Lebesgue measure among sets with the same Lebesgue measure [4]. The coverage function and the Vorob'ev quantiles can be defined similarly for $\mathcal{E}_u^-$.

In a context of Bayesian inference under a Gaussian spatial process prior, references [4, 7, 13, 14, 15] defined alternative descriptors of excursion and contour sets, namely, confidence sets, which we focus on in this paper. In references [7, 13, 14, 15], these confidence sets were defined without reference to the aforementionned descriptors of the random set theory. Azzimonti [4] first revisited confidence sets based on the random set theory. Here, we follow this approach and introduce these confidence sets equivalently with the help of the containment and inclusion functionals of the random set theory. A closed subset $C_{u^+,\alpha}^{\mathrm{out}}$ of D is an outer confidence set for $\mathcal{E}_u^+$ with a probability of at least α if

$$C_{\mathcal{E}_u^+}(C_{u^+,\alpha}^{\mathrm{out}}) \geq \alpha, \tag{3.8}$$

and an open set $C_{u^+,\alpha}^{\mathrm{in}}$ of D is an inner confidence set for $\mathcal{E}_u^+$ with a probability of at least α if

$$I_{\mathcal{E}_u^+}(\mathrm{cl}(C_{u^+,\alpha}^{\mathrm{in}})) \geq \alpha. \tag{3.9}$$

Thus, an outer confidence set $C_{u^+,\alpha}^{\mathrm{out}}$ is such that with a (joint) probability of at least α, it contains all locations where the value taken by the random field exceeds u simultaneously. And, an inner confidence set $C_{u^+,\alpha}^{\mathrm{in}}$ is such that with a (joint) probability of at least α, the value taken by the random field exceeds u for all locations in $C_{u^+,\alpha}^{\mathrm{in}}$ simultaneously. See Fig. 1 for a conceptual diagram of these confidence sets. An outer confidence set $C_{u^-,\alpha}^{\mathrm{out}}$ and an inner confidence set $C_{u^-,\alpha}^{\mathrm{in}}$ can be defined similarly for $\mathcal{E}_u^-$. A closed subset $C_{u^0,\alpha}$ of D is a confidence set for $\mathcal{E}_u^0$ with a probability of at least α if

$$C_{\mathcal{E}_u^0}(C_{u^0,\alpha}) \geq \alpha. \tag{3.10}$$

Thus, a confidence set $C_{u^0,\alpha}$ for $\mathcal{E}_u^0$ is such that with a (joint) probability of at least α, it contains all locations where the value taken by the random field attains u simultaneously. It

can be shown [14] that if $C^{\text{out}}_{u^+,\alpha}$ and $C^{\text{out}}_{u^-,\alpha}$ are outer confidence sets for $\mathcal{E}^+_u$ and $\mathcal{E}^-_u$, respectively, with a probability of at least α, then their complements in $\text{int}(D)$ are inner confidence sets for $\mathcal{E}^-_u$ and $\mathcal{E}^+_u$, respectively, with a probability of at least α. When $\mathcal{E}^0_u \subset \partial\mathcal{E}^+_u$, confidence sets for contour sets can be determined from confidence sets of related excursion sets. For instance, the set

$$C^{\text{out}}_{u^+,\beta} \cap (C^{\text{in}}_{u^+,\beta})^{\text{c}}, \quad \beta \geq \frac{1}{2}(\alpha + 1), \tag{3.11}$$

and the set

$$(N^{\text{in}}_{u^+,\alpha} \cup N^{\text{in}}_{u^-,\alpha})^{\text{c}}, \tag{3.12}$$

with $N^{\text{in}}_{u^+,\alpha}$ and $N^{\text{in}}_{u^-,\alpha}$ in $\mathfrak{L}$ that satisfy $\mathbb{P}(\text{cl}(N^{\text{in}}_{u^+,\alpha}) \subset \mathcal{E}^+_u, \text{cl}(N^{\text{in}}_{u^-,\alpha}) \subset \mathcal{E}^-_u) \geq \alpha$, are both confidence sets for $\mathcal{E}^0_u$ with a probability of at least α.

For the sake of brevity and without loss of generality, we will focus the discussion to follow (mostly) on the construction of an inner confidence set for the positive excursion set.

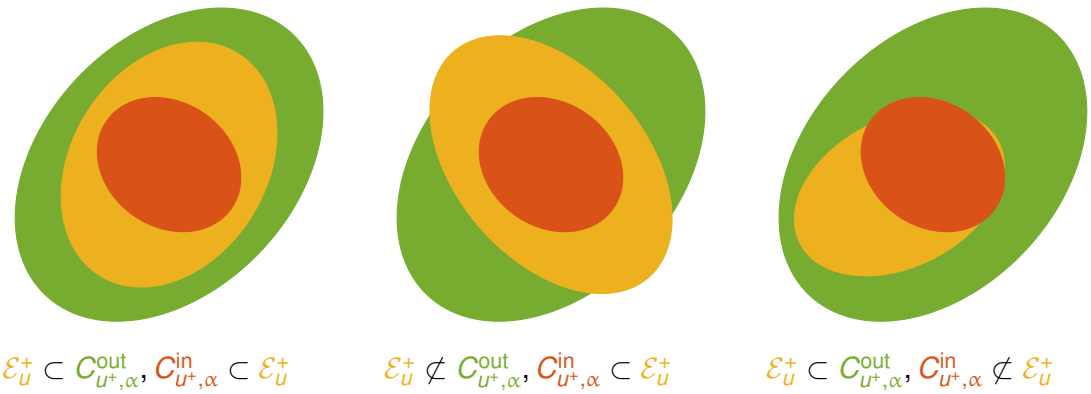

Figure 1. *Conceptual diagram of an outer confidence set $C^{\text{out}}_{u^+,\alpha}$ and an inner confidence set $C^{\text{in}}_{u^+,\alpha}$ for the positive excursion set $\mathcal{E}^+_u$.*

3.2. Optimization within a parametric family. The confidence sets defined above are in general not unique. To determine such confidence sets uniquely, additional restrictions must be imposed. In [4, 7, 14], uniqueness is obtained by first defining a parametric family of candidate sets and then seeking in this family the largest or the smallest set satisfying the joint probability of exceedance constraint. In [4, 7, 14], the family of candidate sets is taken as a parametric family of sets T_ρ indexed by a real number ρ in $(0, 1)$ such that

$$T_\rho = \{\boldsymbol{x} \in \text{int}(D) : T(\boldsymbol{x}) > \rho\}, \tag{3.13}$$

where T is a function from D into $[0, 1]$, also referred to as the membership function by analogy with fuzzy theory. Please note that the membership function T, the candidate sets, and other symbols defined in the following depend on the threshold u, but for the sake of

readability and conciseness, we do not write this dependence explicitly for these new symbols. The membership function is assumed to be continuous in $\mathrm{int}(D)$ so as to ensure that the sets T_ρ belong to $\mathfrak{L}$. Clearly, such a parametric family is nested, that is, $T_\rho \subset T_\sigma$ for $\sigma \leq \rho$. Seeking in this parametric family the largest set satisfying the required joint probability of exceedance constraint amounts to the optimization problem

$$\rho^* = \inf_{\rho\in(0,1)} \rho \text{ subject to } I_{\mathcal{E}_u^+}(\mathrm{cl}(T_\rho)) \geq \alpha, \tag{3.14}$$

with the optimal threshold ρ^* leading to the identification of T_{ρ^*} as the largest inner confidence set with a probability of a least α in the parametric family. For outer confidence sets, one may seek similarly the smallest set in a parametric family.

3.2.1. Choice of the membership function. The definition in (3.13) uses a generic membership function T. For the purpose of constructing confidence sets for the positive excursion set, references [4, 7, 14] suggested and used the following membership functions:

$$T_1(\boldsymbol{x}) = \mathbb{P}(Y(\boldsymbol{x}) \geq u), \tag{3.15}$$

$$T_2(\boldsymbol{x}) = \frac{1}{2}\left(1 + \mathrm{erf}\left(\frac{\mathbb{E}[Y(\boldsymbol{x})] - u}{\sqrt{2\mathbb{V}[Y(\boldsymbol{x})]}}\right)\right), \tag{3.16}$$

$$T_3(\boldsymbol{x}) = \frac{1}{2}\left(1 + \frac{\mathbb{E}[Y(\boldsymbol{x})] - u}{\sqrt{\mathbb{E}[(Y(\boldsymbol{x}) - u)^2]}}\right), \tag{3.17}$$

where $\mathbb{E}$ denotes the mathematical expectation, $\mathbb{V}$ the variance, and erf the error function. Reference [14] argued that the functions in (3.15)–(3.17) are suitable choices for the membership function because they quantify the difference between the value taken by the random field at a location and the threshold u and they account for an associated measure of uncertainty for this difference. The membership function T_1 is the coverage function defined in (3.6) so that the corresponding sets in the parametric family are open Vorob'ev quantiles. The membership functions T_2 and T_3, whose use requires the random field to be of the second order, are transformations of the pointwise difference between the expectation of the random field and the threshold u normalized respectively by the variance of the random field and the expected squared deviation of the random field about the threshold u. If the pointwise (marginal) probability distribution of the random field is Gaussian, then T_1 and T_2 are equal. In addition, when u is zero, as will be the case in the illustration in sect. 6, T_2 and T_3 may be expressed only as a function of the pointwise coefficient of variation $\delta_Y(\boldsymbol{x})$ of the random field:

$$T_2(\boldsymbol{x}) = \frac{1}{2}\left(1 + \mathrm{erf}\left(\frac{1}{\sqrt{2}\delta_Y(\boldsymbol{x})}\right)\right), \tag{3.18}$$

$$T_3(\boldsymbol{x}) = \frac{1}{2}\left(1 + \frac{\mathrm{sgn}(\delta_Y(\boldsymbol{x}))}{\sqrt{\delta_Y^2(\boldsymbol{x}) + 1}}\right), \tag{3.19}$$

where sgn is the sign function, equal to 1 if $\delta_Y(\boldsymbol{x}) \geq 0$ and -1 otherwise.

3.2.2. Interpretation. The membership functions (3.15)–(3.17) are based on pointwise statistical descriptors of the random field. As such, they quantify in some way the pointwise probability of exceeding u in all locations in D individually but do not quantify the joint probability of exceeding u simultaneously at all locations in T_ρ. For instance, the probability of exceeding u simultaneously at all locations in the Vorob'ev ρ-quantile is at most ρ, with a probability of ρ that is achieved when the description of the random field reduces to the description of a single random variable. To achieve the desired confidence level, the threshold ρ^* is determined following the optimization problem (3.14).

The membership function may also be interpreted in the context of the fuzzy set theory [16, 22]. In the fuzzy set theory, any continuous membership function T can be written as $T(\boldsymbol{x}) = \mu(\boldsymbol{x} \in \mathcal{E}_u^+)$, where μ is a fuzzy measure defined on $(\Theta, \mathfrak{B})$. The fuzzy measure μ may be interpreted as a subjective degree of belief about the inclusion of a point $\boldsymbol{x}$ in D in the confidence set. The higher the value of T at a point, the higher the probability of being a member of the confidence set irrespective of the confidence level. Taking the probability measure $\mathbb{P}$ as a fuzzy measure gives the coverage function of the random set $\mathcal{E}_u^+$.

3.2.3. Equivalent problem of quantile estimation. Following the approach in [13, 14], the solution of the optimization problem (3.14) may be recast equivalently as a problem of quantile estimation. Indeed:

$$
\begin{aligned}
I_{\mathcal{E}_u^+}(\mathrm{cl}(T_\rho)) &= \mathbb{P}(\mathrm{cl}(T_\rho) \subset \mathcal{E}_u^+) \\
&= \mathbb{P}(T_\rho \subset \mathcal{E}_u^+) \\
&= \mathbb{P}\big(\big(\mathcal{E}_u^+\big)^{\mathrm{c}} \subset T_\rho^{\mathrm{c}}\big) \\
&= \mathbb{P}\big(T(\boldsymbol{x}) \leq \rho, \boldsymbol{x} \in \big(\mathcal{E}_u^+\big)^{\mathrm{c}}\big) \\
&= \mathbb{P}\Big(\sup_{\boldsymbol{x} \in \left(\mathcal{E}_u^+\right)^{\mathrm{c}}} T(\boldsymbol{x}) \leq \rho\Big).
\end{aligned}
\tag{3.20}
$$

In these equations, the fourth equality does not in general follow from the third equality because there is in general no guarantee that $T(\boldsymbol{x}) \leq \rho$ for all $\boldsymbol{x}$ on ∂D. Thus, the behavior of T on ∂D must be excluded in (3.20). This can be achieved, for instance, by assuming either that T achieves its supremum in $\mathrm{int}\big(\big(\mathcal{E}_u^+\big)^{\mathrm{c}}\big)$ or that T vanishes on ∂D. With these considerations, the optimization problem in (3.14) is equivalent to

$$
\rho^* = \inf_{\rho \in (0,1)} \rho \text{ subject to } \mathbb{P}\Big(\sup_{\boldsymbol{x} \in \left(\mathcal{E}_u^+\right)^{\mathrm{c}}} T(\boldsymbol{x}) \leq \rho\Big) \geq \alpha,
\tag{3.21}
$$

that is, the problem of quantile estimation

$$
\rho^* = \inf\{\rho \in (0,1) : F_\chi(\rho) \geq \alpha\} \equiv q_\chi(\alpha),
\tag{3.22}
$$

where F_χ and q_χ are respectively the distribution function and the generalized quantile function of the random variable

$$
\chi = \sup_{\boldsymbol{x} \in \left(\mathcal{E}_u^+\right)^{\mathrm{c}}} T(\boldsymbol{x}).
\tag{3.23}
$$

Please note that the randomness of χ stems from the random closed set $\mathcal{E}_u^+$, hence the set over which the supremum of T is evaluated. Here, q_χ is a generalized quantile function because, in general, F_χ is not necessarily strictly monotone, for instance, when χ is a discrete random variable (see also sect. 4). If χ is a continuous random variable, then F_χ is strictly monotone and the quantile function is the inverse function of F_χ, that is, $q_\chi(\alpha) = F_\chi^{-1}(\alpha)$.

4. Spatial discretization. To be able to compute confidence sets in practice, a discretization is required. In this section, we describe a discretization of the spatial dimension and discuss its impact on the stochastic dimension. Specifically, we describe a spatial discretization that relies on partitioning the spatial domain into subsets and testing the exceedance constraints in representative points in these subsets. The discrete closed sets thus obtained are random closed sets that the theory of random sets [21] refers to as simple random closed sets by the virtue of them taking only a finite number of values. Please note that alternative spatial discretizations could also be considered, such as spatial discretizations based on computational geometry or computational shape optimization, but we do not consider such alternative spatial discretizations here. We will continue to focus the discussion (mostly) on the positive excursion set and related confidence sets, but please note that the extensions to other confidence sets for negative excursion and contour sets can be obtained analogously.

Let $D^h = \{D_i^h\}_{1\leq i\leq N_h}$ be a partition of D into N_h pairwise disjoint nonempty closed subsets of D, with h a positive number that describes the characteristic size of the subsets. If the random field is a solution quantity of a stochastic computational model that is discretized in space by means of a finite-difference scheme, this partition may be taken as a tessellation based on the grid points; if the stochastic computational model is discretized in space by means of a finite-element scheme, this partition may be taken as the mesh.

Let each subset D_i^h be associated with a representative point $\boldsymbol{x}_i^h$ in D_i^h where we test the exceedance constraint and evaluate the membership function. If the random field is a solution quantity of a stochastic computational model that is discretized in space by means of a finite-difference scheme, these representative points may be taken as the grid points; if the stochastic computational model is discretized in space by means of a finite-element scheme, these representative points may be taken as characteristic points of the elements of the mesh, for instance, the centroids of the elements.

With reference to the partitioning, we approximate $\mathcal{E}_u^+$ with $\mathcal{E}_u^{+h}$ (see Fig. 2 for an illustration) described by the binary random vector $\boldsymbol{E}^h = (E_1^h, \ldots, E_{N_h}^h)$ with values in $\{0,1\}^{N_h}$ such that

$$\mathcal{E}_u^{+h} = \bigcup_{E_i^h=1} D_i^h = \bigcup_{i\in\mathcal{I}_u^{+h}} D_i^h, \tag{4.1}$$

where $\mathcal{I}_u^{+h} = \{i : E_i^h = 1\}$ is the random active index set, with

$$E_i^h = \mathbf{1}(Y(\boldsymbol{x}_i^h) \geq u),\ i = 1, \ldots, N_h; \tag{4.2}$$

here, $\mathbf{1}(Y(\boldsymbol{x}_i^h) \geq u)$ is equal to 1 if $Y(\boldsymbol{x}_i^h) \geq u$ and 0 otherwise.

With reference to the partitioning, we seek inner confidence sets of the form of sets de-

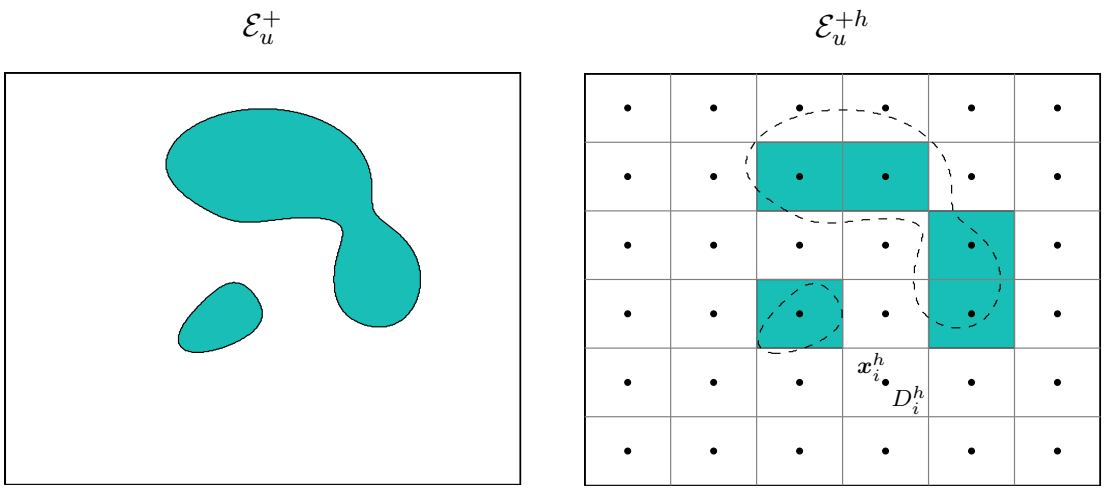

Figure 2. *Illustration of the approximation of the random set $\mathcal{E}_u^+$ as a simple random set $\mathcal{E}_u^{+h}$ based on a structured partitioning of D. The representative points are chosen as the centroids of the elements.*

scribed by a binary vector $\mathbf{c}^h = (c_1^h, \ldots, c_{N_h}^h)$ in $\{0,1\}^{N_h}$ such that

$$C_{u^+,\alpha}^{\mathrm{in,h}} = \mathrm{int}\Big(\bigcup_{c_i^h=1} D_i^h\Big) = \mathrm{int}\Big(\bigcup_{i\in I_{u^+,\alpha}^{\mathrm{in,h}}} D_i^h\Big), \tag{4.3}$$

where $I_{u^+,\alpha}^{\mathrm{in,h}} = \{i : c_i^h = 1\}$ is the active index set. As in the continuous case, we seek such an inner confidence set in a parametric family described by a binary vector $\mathbf{T}_\rho^h = (T_{\rho,1}^h, \ldots, T_{\rho,N_h}^h) = (\mathbf{1}(T_1^h > \rho), \ldots, \mathbf{1}(T_{N_h}^h > \rho))$ in $\{0,1\}^{N_h}$ such that

$$T_\rho^h = \mathrm{int}\Big(\bigcup_{T_{\rho,i}^h=1} D_i^h\Big) = \mathrm{int}\Big(\bigcup_{i\in I_\rho^h} D_i^h\Big), \tag{4.4}$$

where $I_\rho^h = \{i : T_i^h > \rho\}$ is the parametric index set and $\mathbf{T}^h = (T_1^h, \ldots, T_{N_h}^h)$ is the membership vector, with $T_i^h = T(\boldsymbol{x}_i^h)$, $i = 1, \ldots, N_h$.

Seeking the largest set in this parametric family satisfying the joint probability of exceedance constraint associated with the representative points leads to

$$\rho^{*h} = \inf_{\rho\in(0,1)} \rho \text{ subject to } \mathbb{P}\Big(\max_{i\in\left(\mathcal{I}_u^{+h}\right)^{\mathrm{c}}} T_i^h \le \rho\Big) \ge \alpha, \tag{4.5}$$

thus leading to the equivalent problem of quantile estimation

$$\rho^{*h} = \inf\{\rho \in (0,1) : F_{\chi^h}(\rho) \ge \alpha\} \equiv q_{\chi^h}(\alpha), \tag{4.6}$$

where F_{χ^h} and q_{χ^h} are respectively the distribution function and the generalized quantile function of the random variable

$$\chi^h = \max_{i\in\left(\mathcal{I}_u^{+h}\right)^{\mathrm{c}}} T_i^h. \tag{4.7}$$

Due to the approximation of the random closed set as a simple random set, χ^h is a discrete random variable with distinct discrete values $\chi_1^h < \chi_2^h < \ldots < \chi_{L_h}^h$ ($L_h \leq N_h$). In general, L_h is smaller than N_h because there may be locations $\boldsymbol{x}_i^h$ in D where T does not attain its maximum for any realization of $\big(\mathcal{E}_u^{+h}\big)^{\mathrm{c}}$.

The distribution function F_{χ^h} may be written in terms of the probability masses $p_l = \mathbb{P}(\chi^h = \chi_l^h)$, $1 \leq l \leq L_h$, as

$$F_{\chi^h}(\rho) = \mathbb{P}(\chi^h \leq \rho) = \sum_{\chi_l^h \leq \rho} \mathbb{P}(\chi^h = \chi_l^h) = \sum_{\chi_l^h \leq \rho} p_l. \tag{4.8}$$

Then, the problem of quantile estimation reads as

$$\rho^{*h} = \min_{\chi_l^h \in \{\chi_1^h, \ldots, \chi_{L_h}^h\}} \chi_l^h \text{ subject to } \sum_{k=1}^{l} p_k \geq \alpha. \tag{4.9}$$

Thus, the impact of the discretization of the spatial dimension on the stochastic dimension is that both F_{χ^h} and q_{χ^h} are piecewise-constant functions with discontinuities whose number and magnitude depend on the spatial resolution of the computational model. Consequently, the accuracy one may achieve in estimating confidence sets for a spatial discretization of the domain is influenced by the spatial resolution of the computational model. Specifically, the solution ρ^* of (3.22) is always larger than or equal to the solution ρ^{*h} of (4.6), with the difference between both solutions depending on the magnitude of the discontinuities around ρ^*.

Please note that a similar spatial discretization had already been used in reference [14], albeit in a different context, which provided a consistency result:

Proposition 4.1. *Suppose that*

(a) $\exists \epsilon > 0$ *such that*

$$\mathbb{P}\Big[\inf \big\{ \|\boldsymbol{x} - \boldsymbol{x}'\| : \boldsymbol{x} \in \partial T_{\rho^*}, \boldsymbol{x}' \in \partial \mathcal{E}_u^+ \big\} \geq \epsilon \Big| \operatorname{cl}(T_{\rho^*}) \subset \mathcal{E}_u^+ \Big] = 1, \tag{4.10}$$

where $\|\cdot\|$ *is the Euclidean norm;*

(b) the partitions satisfy the following conditions:

1) $\forall N_h, N_{h'} \in \mathbb{N}_0$ *with* $N_{h'} > N_h$, $D^{h'}$ *is a refinement of* D^h *in the particular sense that each subset of* $D^{h'}$ *is a subset of some subset of* D^h*;*

2) $\forall \eta > 0$, $\exists M_\eta \in \mathbb{N}_0 : D_i^h \subset B_\eta(\boldsymbol{x}_i^h)$ *for* $i = 1, \ldots, M_\eta$, *where* $B_\eta(\boldsymbol{x})$ *is a ball of radius* η *centered at* $\boldsymbol{x}$.

Then, $\forall N_h \geq M_{\epsilon/2}$, $I_{\mathcal{E}_u^+}\big(\operatorname{cl}(T_{\rho^{*h}}^h)\big) \geq \alpha$.

Condition (a) states that there is at least a small "buffer" between the boundary of $\mathcal{E}_u^+$ and T_{ρ^*}. Condition (b.1) means that finer partitions are obtained by partitioning subsets of coarser partitions. Condition (b.2) means that all subsets in the partition become arbitrarily small for large enough N_h. Proposition 4.1 ensures that for N_h sufficiently large, an inner confidence set $T_{\rho^{*h}}^h$ for the simple random set $\mathcal{E}_u^{+h}$ in (4.1) for a confidence level α is an inner confidence set for the random closed set $\mathcal{E}_u^+$ for the same confidence level.

5. Discretization of the stochastic dimension. The identification of a confidence set in a parametric family of candidate sets leads to a two-step problem. The first step involves the determination of the membership function, and the second step involves the determination of the appropriate threshold by solving an optimization problem that may be recast equivalently as a quantile estimation problem. The first step requires the approximation of pointwise (marginal) statistical descriptors of the random field, and the second step requires the approximation of joint probabilities of exceedance at all considered locations simultaneously. Because the second step requires the approximation of joint probabilities, it can be expected to be more computationally challenging, and especially so when evaluating whether inclusion relationships hold with high probability levels, which raises the issue of rare events. Hence, while we will provide some details regarding the estimation of pointwise statistical descriptors, we will focus (most of) the discussion to follow on the quantile estimation problem.

In the following, we assume $\{Y(\boldsymbol{x}), \boldsymbol{x} \in D\}$ to be a solution quantity of a stochastic computational model that depends on a finite number of uncertain parameters $\xi_1, \ldots, \xi_n$, modelled as an $\mathbb{R}^n$-valued random vector $\boldsymbol{\xi} = (\xi_1, \ldots, \xi_n)$ defined on $(\Theta, \mathfrak{B}, \mathbb{P})$. In this section, we will not distinguish between χ and χ^h and use the symbol χ as a generic notation for both the continuous random variable χ and its spatial discretization χ^h following sect. 4, and we discuss the impact of the spatial discretization where appropriate.

5.1. Membership function. The membership functions defined in (3.15)–(3.17) involve pointwise (marginal) statistical descriptors of $\{Y(\boldsymbol{x}), \boldsymbol{x} \in D\}$. For each $\boldsymbol{x}$ in D, an approximation of $T(\boldsymbol{x})$ may be obtained by using standard nonintrusive methods for uncertainty quantification. In sect. 6.6, we compute the required approximations to the pointwise (marginal) statistical descriptors of the random field by applying a kernel density estimation method to an ensemble of independent and identically distributed (i.i.d.) samples of the random field, from which we deduce a Monte Carlo approximation of T by using a Monte Carlo sampling of the kernel density estimates. Please note that although the choice of a different membership function or errors entailed by its numerical approximation may change the parametric family of candidate sets, a set satisfying the joint probability of exceedance constraint may still be sought within this parametric family.

5.2. Quantile estimation: Monte Carlo method.

5.2.1. Use of distribution function. An implementation of the Monte Carlo method begins by generating an ensemble of i.i.d. samples $\{\boldsymbol{\xi}(\theta^{(k)}), 1 \leq k \leq \nu\}$ of the uncertain parameters. Then, an ensemble of solutions to the computational model is generated in the form of the ensemble of the corresponding i.i.d. samples of the random field, from which are deduced the ensemble of the corresponding i.i.d. samples $\{\mathcal{E}_u^+(\theta^{(k)}), 1 \leq k \leq \nu\}$ of the excursion set and the ensemble of the corresponding i.i.d. samples $\{\chi(\theta^{(k)}), 1 \leq k \leq \nu\}$ of χ. Then, the sample (empirical) distribution function evaluated at ρ in $(0, 1)$ writes as

$$F_\chi^\nu(\rho) = \frac{1}{\nu} \sum_{k=1}^{\nu} \mathbf{1}\big(\chi(\theta^{(k)}) \leq \rho\big), \tag{5.1}$$

where the superscript ν is used to indicate that the quantity is estimated from a finite number of samples. The corresponding sample quantile $q_\chi^\nu(\alpha)$ is then given by

$$q_\chi^\nu(\alpha) = \inf\left\{\rho \in (0,1) : F_\chi^\nu(\rho) \geq \alpha\right\}. \tag{5.2}$$

Equivalently, this Monte Carlo estimate may be obtained by ordering the i.i.d. samples as $\chi_{1:\nu} \leq \chi_{2:\nu} \leq \ldots \leq \chi_{\nu:\nu}$, where $\chi_{k:\nu}$ denotes the k-th order statistic of the samples [3], that is, $\chi_{1:\nu}$ denotes the smallest sample, $\chi_{2:\nu}$ the second smallest sample, ..., and $\chi_{\nu:\nu}$ the largest sample. Then $q_\chi^\nu(\alpha)$ is given by $\chi_{k:\nu}$, where $(k-1)/\nu < \alpha \leq k/\nu$.

If χ is a continuous random variable with a probability density function, $q_\chi^\nu(\alpha)$ is associated with a consistent estimator of $q_\chi(\alpha)$ that satisfies a central limit theorem [3]. However, if χ is a discrete random variable, then the Monte Carlo estimator is not guaranteed to satisfy a central limit theorem or to be a consistent estimator. The lack of consistency mainly results from the discontinuities of the distribution function, if any, which may cause the problem of quantile estimation to be ill-conditioned because small perturbations in α or F_χ^ν may cause large perturbations in $q_\chi^\nu(\alpha)$. Feldman and Tucker [11] showed that, for an arbitrary distribution function, a sequence of Monte Carlo estimates $\left\{q_\chi^\nu(\alpha)\right\}$ may oscillate between $\inf\{\rho \in (0,1) : F_\chi(\rho) \geq \alpha\}$ and $\sup\{\rho \in (0,1) : F_\chi(\rho) \leq \alpha\}$.

5.2.2. Use of mid-distribution function. If χ is a discrete random variable, an alternative method is to rely on a regularization of the problem of quantile estimation based on the mid-distribution function [20, 23]. Let $\chi_1 < \ldots < \chi_L$ denote the discrete values that χ may take; then the mid-distribution function F_χ^{mid} is the following continuous, piecewise linear modification of the distribution function

$$F_\chi^{\mathrm{mid}}(\rho) = \begin{cases} 0 & \text{if } \rho < \chi_1 \\ \dfrac{F_\chi^{\mathrm{mid}}(\chi_{l+1}) - F_\chi^{\mathrm{mid}}(\chi_l)}{\chi_{l+1} - \chi_l}(\rho - \chi_l) + F_\chi^{\mathrm{mid}}(\chi_l) & \text{if } \chi_l \leq \rho \leq \chi_{l+1}, \\ 1 & \text{if } \rho > \chi_L \end{cases} \tag{5.3}$$

where $F_\chi^{\mathrm{mid}}(\chi_l) = F_\chi(\chi_l) - \frac{1}{2}p_\chi(\chi_l)$ for $1 \leq l \leq L$, with $p_\chi(\rho) = \mathbb{P}(\chi = \rho)$ the probability mass function. The corresponding mid-quantile function is then a continuous, piecewise linear modification of the quantile function given by

$$q_\chi^{\mathrm{mid}}(\alpha) = \inf\left\{\rho \in (0,1) : F_\chi^{\mathrm{mid}}(\rho) \geq \alpha\right\}. \tag{5.4}$$

The Monte Carlo estimate $q_\chi^{\mathrm{mid},\nu}(\alpha)$ of $q_\chi^{\mathrm{mid}}(\alpha)$ is given by

$$q_\chi^{\mathrm{mid},\nu}(\alpha) = \inf\left\{\rho \in (0,1) : F_\chi^{\mathrm{mid},\nu}(\rho) \geq \alpha\right\}, \tag{5.5}$$

where the sample mid-distribution function is given by

$$F_\chi^{\mathrm{mid},\nu}(\rho) = \begin{cases} 0 & \text{if } \rho < \chi_1 \\ \dfrac{F_\chi^{\mathrm{mid},\nu}(\chi_{l+1}) - F_\chi^{\mathrm{mid},\nu}(\chi_l)}{\chi_{l+1} - \chi_l}(\rho - \chi_l) + F_\chi^{\mathrm{mid},\nu}(\chi_l) & \text{if } \chi_l \leq \rho \leq \chi_{l+1}, \\ 1 & \text{if } \rho > \chi_L \end{cases} \tag{5.6}$$

with

$$F_\chi^{\mathrm{mid},\nu}(\chi_l) = \frac{1}{\nu}\sum_{k=1}^{\nu}\mathbf{1}\big(\chi(\theta^{(k)}) \le \chi_l\big) - \frac{1}{2\nu}\sum_{k=1}^{\nu}\mathbf{1}\big(\chi(\theta^{(k)}) = \chi_l\big),\ 1 \le l \le L. \tag{5.7}$$

Ma et al. [20] have shown that $q_\chi^{\mathrm{mid},\nu}(\alpha)$ is associated with a consistent estimator of $q_\chi^{\mathrm{mid}}(\alpha)$ that satisfies a generalized central limit theorem. However, $q_\chi^{\mathrm{mid},\nu}(\alpha)$ is not guaranteed to be associated with a consistent estimator of $q_\chi(\alpha)$ because $q_\chi^{\mathrm{mid}}(\alpha)$ may be different from $q_\chi(\alpha)$. Yet, the difference between $q_\chi(\alpha)$ and $q_\chi^{\mathrm{mid}}(\alpha)$ may be expected to tend to zero as the set of discrete values taken by χ becomes denser and denser as L tends to infinity.

5.2.3. Computational cost. The Monte Carlo estimator based on the distribution function for continuous χ entails an approximation error that decreases with the square root of the number of samples ν and increases with the ratio of the square root of $\alpha(1-\alpha)$ and the value taken by the probability density function of χ at the quantile to be estimated; for the Monte Carlo estimator based on the mid-distribution function for discrete χ, there exists an analogous result that involves a generalised notion of probability density function [20]. Thus, attaining sufficient accuracy may become intractable for computational models with a high computational cost and for quantiles associated with low and high levels of probability (rare events).

5.3. Quantile estimation: spectral method. We propose two methods that seek to alleviate the computational cost via the construction of a surrogate model.

5.3.1. Spectral representation of the random field. The first method involves building a polynomial chaos expansion of $\{Y(\boldsymbol{x}), \boldsymbol{x} \in D\}$ and then using this polynomial chaos expansion as a substitute for evaluations of the computational model when solving the quantile estimation problem. A truncated polynomial chaos expansion of order p of the random field, assumed to be of the second order, writes as

$$Y^p(\boldsymbol{x}) = \sum_{|\boldsymbol{\alpha}|=0}^{p} y_{\boldsymbol{\alpha}}^p(\boldsymbol{x})\,\psi_{\boldsymbol{\alpha}}(\boldsymbol{\xi}). \tag{5.8}$$

Here, $\boldsymbol{\alpha} = (\alpha_1, \ldots, \alpha_n)$ is a multi-index with $|\boldsymbol{\alpha}| = \alpha_1 + \ldots + \alpha_n$ and $\{\psi_{\boldsymbol{\alpha}}, \boldsymbol{\alpha} \in \mathbb{N}^n\}$ is a suitable basis of orthogonal polynomials from $\mathbb{R}^n$ into $\mathbb{R}$. The functions $y_{\boldsymbol{\alpha}}^p$ from D into $\mathbb{R}$ are the polynomial chaos coordinates. In practice, these polynomial chaos coordinates may be determined by using nonintrusive methods from solutions of the computational model for an experimental design of the uncertain parameters denoted by $\big\{\boldsymbol{\xi}(\theta_\lambda^{(k)}), 1 \le k \le \lambda\big\}$.

The random set $\mathcal{E}_u^+$ is then approximated with the corresponding excursion set determined with the polynomial chaos expansion, that is,

$$\mathcal{E}_u^{+,p} = \{\boldsymbol{x} \in D : Y^p(\boldsymbol{x}) \ge 0\}, \tag{5.9}$$

and χ is approximated with

$$\sup_{\boldsymbol{x} \in \left(\mathcal{E}_u^{+,p}\right)^c} T(\boldsymbol{x}). \tag{5.10}$$

This first method amounts to approximating a confidence set for the excursion set of $\{Y(\boldsymbol{x}), \boldsymbol{x} \in D\}$ with the corresponding confidence set for the excursion set of $\{Y^p(\boldsymbol{x}), \boldsymbol{x} \in D\}$. The confidence set can then be evaluated by using either formalism (3.14), with $\mathcal{E}_u^+$ approximated with $\mathcal{E}_u^{+,p}$, or formalism (3.22), with F_χ approximated with a Monte Carlo estimate as

$$\frac{1}{\nu}\sum_{k=1}^{\nu} \mathbf{1}\Big(\sup_{\boldsymbol{x}\in\big(\mathcal{E}_u^{+,p}(\theta^{(k)})\big)^{\mathrm{c}}} T(\boldsymbol{x}) \leq \rho \Big). \tag{5.11}$$

5.3.2. Spectral representation of the random variable χ. The second method, enabled by the reformulation of the optimization problem in (3.14) as the quantile estimation problem in (3.22), involves building a polynomial chaos expansion directly of χ. A truncated polynomial chaos expansion of order p of χ, assumed to be of the second order, writes as

$$\chi^p = \sum_{|\boldsymbol{\alpha}|=0}^{p} \chi^p_{\boldsymbol{\alpha}}\, \psi_{\boldsymbol{\alpha}}(\boldsymbol{\xi}), \tag{5.12}$$

where the scalars $\chi^p_{\boldsymbol{\alpha}}$ are the polynomial chaos coordinates. In practice, these polynomial chaos coordinates may be determined by using nonintrusive methods from solutions of the computational model for an experimental design of the uncertain parameters denoted by $\big\{\boldsymbol{\xi}(\theta_\lambda^{(k)}), 1 \leq k \leq \lambda\big\}$. The confidence set can then be evaluated using formalism (3.22), with F_χ approximated with a Monte Carlo estimate as

$$\frac{1}{\nu}\sum_{k=1}^{\nu} \mathbf{1}\big(\chi^p(\theta^{(k)}) \leq \rho\big). \tag{5.13}$$

Whereas the accuracy of the spectral representation depended in the previous section on how well $\{Y(\boldsymbol{x}), \boldsymbol{x} \in D\}$ lends itself to being approximated with a truncated polynomial chaos expansion, the accuracy of the spectral representation depends here on how well χ lends itself to being approximated with a truncated polynomial chaos expansion. The choice of the membership function plays a role in this issue, which we will study numerically later in the illustration in sect. 6.

5.3.3. Surrogate-based quantile estimation. The use of a truncated polynomial chaos expansion as in (5.8) or (5.12) as an approximation to $\{Y(\boldsymbol{x}), \boldsymbol{x} \in D\}$ or χ in the quantile estimation may lead to an approximation error, which obeys the following result from [10, 18]:

Theorem 5.1. *Let χ and $\widetilde{\chi}$ be random variables with values in $\mathbb{R}$ and α a scalar in $(0,1)$. Let $\delta > 0$ be such that*

$$|\widetilde{\chi} - \chi| \leq \frac{\delta}{2} + \frac{1}{2}|q_\chi(\alpha) - \chi|, \tag{5.14}$$

almost surely. Then, the error in approximating $q_\chi(\alpha)$ with $q_{\widetilde{\chi}}(\alpha)$ satisfies

$$|q_{\widetilde{\chi}}(\alpha) - q_\chi(\alpha)| \leq \delta. \tag{5.15}$$

Here, we use the notation $\widetilde{\chi}$ to denote a generic surrogate model that could be obtained based on (5.8) or (5.12), and we will continue to use this notation throughout the remainder of this section. Please note that a similar result may be obtained for quantile estimation using the mid-distribution function. Theorem 5.1 provides for the error between $q_{\widetilde{\chi}}(\alpha)$ and $q_\chi(\alpha)$ an error bound δ that depends on the local approximation error $|\widetilde{\chi} - \chi|$ between χ and its surrogate and on the distance $|q_\chi(\alpha) - \chi|$ between the quantile to be estimated and χ. Hence, one may seek to reduce the value of δ by lowering the local approximation error where χ is close to $q_\chi(\alpha)$, while the surrogate model does not need to be a good approximation to χ further away from the quantile to be estimated.

5.3.4. Computational cost. The computational cost of constructing a truncated polynomial chaos expansion as in (5.8) or (5.12) depends on the order p; the higher the order p must be to attain sufficient accuracy, the higher the number of training points must be in the experimental design. This computational cost also scales with the number of uncertain parameters (the stochastic dimension n); the higher the stochastic dimension n, the higher the number of required training points may be expected to be in the experimental design.

5.4. Quantile estimation: bifidelity method. By writing the distribution function F_χ in (3.22) of the random variable χ in (3.23) as

$$F_\chi(\rho) = \mathbb{P}(\chi \leq \rho) = \int_{\Theta_\rho} d\mathbb{P}(\theta) = \int_\Theta \mathbf{1}(\theta \in \Theta_\rho) d\mathbb{P}(\theta), \tag{5.16}$$

it can be seen that the solution of the quantile estimation problem is related to the fundamental problem of reliability engineering of evaluating the probability of an event $\Theta_\rho = \{\theta \in \Theta : \chi(\theta) - \rho \leq 0\}$ defined by a limit state function, also called performance function, here, $\chi - \rho$. In reliability engineering, methods have been developed for the efficient approximation of such probabilities, such as methods using surrogate models, subset simulation, and other methods. Hence, we will build on a hybrid method introduced in [19] in reliability engineering to develop a new bifidelity method that can reduce the number of samples of the stochastic computational model that must be solved.

5.4.1. Method. Conceptually, this method relies on a bifidelity model that combines a surrogate model, such as one of those discussed in sect. 5.3, with the computational model. The surrogate model is used further away from the quantile to be estimated, and the computational model is used closer to the quantile to be estimated:

$$\widetilde{\chi}^\gamma = \widetilde{\chi}\, \mathbf{1}\left(|\widetilde{\chi} - q_\chi(\alpha)| > \gamma\right) + \chi\, \mathbf{1}\left(|\widetilde{\chi} - q_\chi(\alpha)| \leq \gamma\right), \tag{5.17}$$

where $\widetilde{\chi}$ is the surrogate model of χ and $\gamma > 0$ is a threshold parameter that controls the size of the region in the parameter space where χ is used. From (5.17), we see that the local approximation error $|\widetilde{\chi}^\gamma - \chi|$ vanishes where $|\widetilde{\chi} - q_\chi(\alpha)| \leq \gamma$. Therefore, the error bound δ in (5.14) may be expected to decrease with an increase in γ.

By adapting Theorem 4.1 stated in [19] for the computation of failure probabilities, the following result is obtained as an error estimate for the quantile estimation problem:

Theorem 5.2. *Let χ and $\widetilde{\chi}$ be random variables with values in $\mathbb{R}$, and let $\widetilde{\chi}^\gamma$ be defined as in (5.17) with γ that satisfies*

$$\mathbb{P}\left(|\widetilde{\chi}-\chi|>\gamma\right)\leq\epsilon \tag{5.18}$$

for some $\epsilon\geq 0$. Then, the quantile function $q_{\widetilde{\chi}^\gamma}$ satisfies

$$q_{\widetilde{\chi}^\gamma}(\alpha-\epsilon)\leq q_\chi(\alpha)\leq q_{\widetilde{\chi}^\gamma}(\alpha+\epsilon). \tag{5.19}$$

Proof. We consider the following inequality

$$\mathbb{P}\Big(\widetilde{\chi}^\gamma\leq q_\chi(\alpha)\Big)\geq\mathbb{P}\Big(\chi\leq q_\chi(\alpha)\Big)-\mathbb{P}\Big(\widetilde{\chi}^\gamma>q_\chi(\alpha),\chi\leq q_\chi(\alpha)\Big). \tag{5.20}$$

The last event is possible only if $|\widetilde{\chi}-q_\chi(\alpha)|>\gamma$. Then, we have

$$\begin{aligned}\mathbb{P}\Big(\widetilde{\chi}^\gamma>q_\chi(\alpha),\chi\leq q_\chi(\alpha)\Big)&=\mathbb{P}\Big(\widetilde{\chi}-q_\chi(\alpha)>\gamma,\chi\leq q_\chi(\alpha)\Big)\\&\leq\mathbb{P}\Big(\widetilde{\chi}-\chi>\gamma\Big)\\&\leq\epsilon.\end{aligned} \tag{5.21}$$

Therefore, inequality (5.20) becomes

$$F_{\widetilde{\chi}^\gamma}(q_\chi(\alpha))\geq F_\chi(q_\chi(\alpha))-\epsilon=\alpha-\epsilon, \tag{5.22}$$

that is, the infimum of $\widetilde{\chi}^\gamma$ for which $F_{\widetilde{\chi}^\gamma}$ is equal to or exceeds $\alpha-\epsilon$ is at most $q_\chi(\alpha)$. Hence,

$$q_{\widetilde{\chi}^\gamma}(\alpha-\epsilon)=\inf\left\{\rho\in(0,1):F_{\widetilde{\chi}^\gamma}(\rho)\geq\alpha-\epsilon\right\}\leq q_\chi(\alpha). \tag{5.23}$$

Similarly, we can show that

$$F_{\widetilde{\chi}^\gamma}(q_\chi(\alpha))\leq F_\chi(q_\chi(\alpha))+\epsilon=\alpha+\epsilon, \tag{5.24}$$

that is, the infimum of $\widetilde{\chi}^\gamma$ for which $F_{\widetilde{\chi}^\gamma}$ is equal to or exceeds $\alpha+\epsilon$ is at least $q_\chi(\alpha)$. Hence,

$$q_{\widetilde{\chi}^\gamma}(\alpha+\epsilon)=\inf\left\{\rho\in(0,1):F_{\widetilde{\chi}^\gamma}(\rho)\geq\alpha+\epsilon\right\}\geq q_\chi(\alpha). \tag{5.25}$$

■

The value of the threshold γ required to achieve a level of accuracy ϵ depends on the approximation error between χ and its surrogate model $\widetilde{\chi}$. Proposition 5.3 by [19] gives a lower bound on the threshold parameter γ when the $\mathbb{L}^q$-error between χ and $\widetilde{\chi}$ is bounded:

Proposition 5.3. *Let χ and $\widetilde{\chi}$ be random variables with values in $\mathbb{R}$ and q a scalar with $q\geq 1$ such that*

$$\|\chi-\widetilde{\chi}\|_{\mathbb{L}^q}=\left(\mathbb{E}(|\chi-\widetilde{\chi}|^q)\right)^{1/q}<\infty. \tag{5.26}$$

Then for all $\epsilon>0$, there exists $\gamma^*>0$ such that for all $\gamma\geq\gamma^*$:

$$\mathbb{P}\left(|\widetilde{\chi}-\chi|>\gamma\right)\leq\epsilon; \tag{5.27}$$

more precisely,

$$\gamma^*=\frac{1}{\epsilon^{1/q}}\|\chi-\widetilde{\chi}\|_{\mathbb{L}^q}. \tag{5.28}$$

5.4.2. Implementation. The construction of the bifidelity model (5.17) requires knowing the quantile $q_\chi(\alpha)$ and the threshold parameter γ, which depends on the $\mathbb{L}^q$-error between χ and $\widetilde{\chi}$. The quantile $q_\chi(\alpha)$ and the approximation error are in general not known *a priori*. Following [19], one can use a constructive iterative algorithm that does not require the *a priori* choice of γ (Algorithm 5.1). To initialize this algorithm, a number ν of i.i.d. samples of the uncertain parameters is simulated, a surrogate model $\widetilde{\chi}$ is built, and a small positive parameter η is chosen for setting a stopping criterion. At each iteration j, the sample set S is divided into a set $\widetilde{S}^{(j)}$ of samples for which $\widetilde{\chi}$ is evaluated and a set $S \setminus \widetilde{S}^{(j)}$ for which χ is evaluated. In the initialization step, $\widetilde{S}^{(0)} = S$ and an initial estimate of the quantile is determined by using only $\widetilde{\chi}$. At each iteration j, the set $S \setminus \widetilde{S}^{(j)}$ is determined by enriching the set $S \setminus \widetilde{S}^{(j-1)}$ with the $\Delta\nu$ samples in $\widetilde{S}^{(j-1)}$ that are closest to the current quantile estimate and a new quantile estimate is evaluated by using the updated bifidelity model

$$\widetilde{\chi}^{\gamma}(\theta^{(k)}) = \widetilde{\chi}(\theta^{(k)})\,\mathbf{1}\big(\boldsymbol{\xi}(\theta^{(k)}) \in \widetilde{S}^{(j)}\big) + \chi(\theta^{(k)})\,\mathbf{1}\big(\boldsymbol{\xi}(\theta^{(k)}) \in (S \setminus \widetilde{S}^{(j)})\big), \quad 1 \le k \le \nu. \tag{5.29}$$

Algorithm 5.1 Iterative algorithm for the bifidelity method

Initialization:

1. Build a surrogate model $\widetilde{\chi}$ of χ.
2. Draw ν i.i.d. samples to obtain $S = \{\boldsymbol{\xi}(\theta^{(k)}), 1 \le k \le \nu\}$.
3. Set $k = 0$, $\widetilde{S}^{(0)} = S$, $\Delta\nu \ll \nu$ (step size), and $\eta \ge 0$ (small number).
4. Evaluate $\{\widetilde{\chi}(\theta^{(k)}), 1 \le k \le \nu\}$.
5. Set $q^{(0)}(\alpha)$ as the α-quantile of $\{\widetilde{\chi}(\theta^{(k)}), 1 \le k \le \nu\}$.

Iteration: at the j-th iteration ($j \ge 1$), **do**:

1. Sort $\left\{|\widetilde{\chi}(\theta^{(k)}) - q^{(j-1)}(\alpha)|, \theta^{(k)} \in \widetilde{S}^{(j-1)}\right\}$ in ascending order.
   Let $\Delta\widetilde{S}^{(j)}$ collect the $\Delta\nu$ smallest elements and $\widetilde{S}^{(j)} = \widetilde{S}^{(j-1)} \setminus \Delta\widetilde{S}^{(j)}$.
2. Evaluate $\chi(\theta^{(k)})$ and replace $\widetilde{\chi}(\theta^{(k)})$ with $\chi(\theta^{(k)})$, $\forall \theta^{(k)} \in \Delta\widetilde{S}^{(j)}$.
3. Set $q^{(j)}(\alpha)$ as the α-quantile of $\{\widetilde{\chi}(\theta^{(k)}), 1 \le k \le \nu\}$.
4. If $|q^{(j)}(\alpha) - q^{(j-1)}(\alpha)| \le \eta$ or $\widetilde{S}^{(j)} = \emptyset$, exit; otherwise increment j by 1.

Return $q^{(j)}(\alpha)$ as an estimate of $q_\chi(\alpha)$.

5.4.3. Computational cost. In addition to the computational cost of constructing a truncated polynomial chaos expansion as in (5.8) or (5.12), the accuracy and efficiency of Algorithm 5.1 depend on the stopping criterion and the step size $\Delta\nu$. In principle, the algorithm will converge to the Monte Carlo estimate once all the samples are evaluated with the computational model. In practice, it is desirable to stop the algorithm before this point to reduce the number of evaluations of the computational model. Nevertheless, while a stopping criterion implies the numerical convergence of the quantile estimate, it may not guarantee the convergence towards the quantile to be estimated. Thus, the accuracy of the surrogate model may be expected to have a direct impact on the efficiency of the algorithm. A small step size may be expected to be more optimal in terms of the total number of evaluations of the computational model but to converge in more iterations, while a higher step size may be expected to be less optimal in terms of the total number of evaluations of the computational model but

to converge in less iterations. At each iteration, the $\Delta\nu$ new evaluations of the computational model may be performed in parallel depending on the available computational resources.

6. Application: Uncertainty quantification of Antarctic ice-sheet retreat.

6.1. Context. A key challenge in assessing future sea-level rise stems from assessing the contribution of the AIS, whose response is expected to be dominated by the evolution of its marine sectors. Marine sectors are portions of the ice sheet where the ice is grounded, that is, rests on bedrock, below sea level and extends into floating ice shelves at the grounding line, the transition line where the ice becomes afloat. Such marine sectors, such as those in the West Antarctic ice sheet (WAIS), might retreat significantly in the next decades and centuries as a consequence of an instability mechanism, the so-called marine ice-sheet instability [26]. Therefore, a significant interest in glaciology is directed towards quantifying the retreat of marine sectors and determining the position of the grounding line, as a way of assessing the vulnerability of the AIS to climate change; see, for instance, [8, 25, 28].

6.2. Computational ice-sheet model. We use the fast Elementary Thermomechanical Ice Sheet (f.ETISh) model, a computational ice-sheet model that reduces the three-dimensional nature of ice-sheet flow to a two-dimensional problem while keeping the essential characteristics of ice-sheet thermodynamics and ice-stream flow [24]. Prescribed fields and data include present-day ice-sheet geometry and topography, the basal sliding coefficient inferred with a data assimilation method, present-day atmospheric temperature and precipitation, and present-day ocean temperature. Processes controlling grounding-line motion are taken into account in such a way that they can be represented at coarser resolutions. The discretization of space is a finite-difference discretization on staggered grids and the discretization of time is implicit.

6.3. Initial boundary value problem. The f.ETISh model solves a nonlinear initial boundary value problem that is defined on a spatial domain taken as a closed subset D of $\mathbb{R}^2$. This spatial domain D is assumed to be covered with ice at all times. At any time $0 < t < \tau$, $D_{\mathrm{g}}(t)$ represents the closed subset of D where the ice is grounded and $D_{\mathrm{f}}(t)$ represents the closed subset of D where the ice is floating (Fig. 3). At any time, ∂D belongs to the boundary ∂D_{f} of D_{f}. The grounding line is given by $\Gamma = D_{\mathrm{g}} \cap D_{\mathrm{f}}$.

The f.ETISh model solves a coupled thermo-mechanical system of equations for the ice velocity $\mathbf{v}$, the ice thickness h, the ice temperature T, and the bedrock elevation b measured with respect to sea level. For a comprehensive overview of the governing equations, we refer to [24]. As described in [24], the ice velocity and the ice thickness are obtained by solving a hybrid combination of governing equations according to the shallow-ice approximation and governing equations according to the shallow-shelf approximation. Here, in order to provide essential insight and allow us to present later in the paper the sources of the uncertainty, we limit ourselves to presenting only the governing equations according to the shallow-shelf

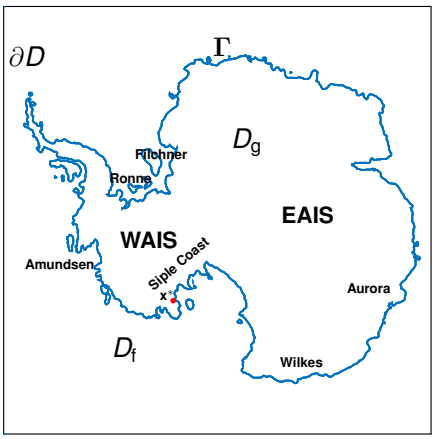

Figure 3. *Current configuration of the AIS with key geographic sectors in bold type. The ice is grounded on the bedrock in D_g and floating in D_f. The separation line Γ between D_g and D_f is the grounding line.* ***WAIS*** *is the West Antarctic ice sheet and* ***EAIS*** *is the East Antarctic ice sheet.*

approximation. For $0 < t < \tau$, the ice-sheet dynamics is described by the following system:

$$\begin{cases} \dfrac{\partial h}{\partial t} + \mathrm{div}_{\boldsymbol{x}}(h\mathbf{v}) = a_{\mathrm{s}}(T_{\mathrm{a}}) - a_{\mathrm{b}} \\ \mathrm{div}_{\boldsymbol{x}}\left(2\eta_{\mathrm{e}} h\left[\mathbf{D}(\mathbf{v}) + \mathrm{tr}\left(\mathbf{D}(\mathbf{v})\right)\mathbf{I}\right]\right) - c_{\mathrm{b}}\left|\mathbf{v}\right|^{m-1}\mathbf{v} - \rho_{\mathrm{i}} g h \nabla_{\boldsymbol{x}}(b+h) = \mathbf{0} \ \text{ in } \mathrm{int}(D_{\mathrm{g}}), \\ h > -\dfrac{\rho_{\mathrm{w}}}{\rho_{\mathrm{i}}} b \end{cases} \tag{6.1}$$

$$\begin{cases} \dfrac{\partial h}{\partial t} + \mathrm{div}_{\boldsymbol{x}}(h\mathbf{v}) = a_{\mathrm{s}}(T_{\mathrm{a}}) - a_{\mathrm{w}}(T_{\mathrm{o}}) \\ \mathrm{div}_{\boldsymbol{x}}\left(2\eta_{\mathrm{e}} h\left[\mathbf{D}(\mathbf{v}) + \mathrm{tr}\left(\mathbf{D}(\mathbf{v})\right)\mathbf{I}\right]\right) - \dfrac{1}{2}\left(1 - \dfrac{\rho_{\mathrm{i}}}{\rho_{\mathrm{w}}}\right)\rho_{\mathrm{i}} g \nabla_{\boldsymbol{x}} h^2 = \mathbf{0} \ \text{ in } \mathrm{int}(D_{\mathrm{f}}), \\ h < -\dfrac{\rho_{\mathrm{w}}}{\rho_{\mathrm{i}}} b \end{cases} \tag{6.2}$$

$$\text{Transmission conditions across } \Gamma. \tag{6.3}$$

Here, $\mathbf{D}(\mathbf{v})$ is the horizontal strain-rate tensor, $\mathbf{I}$ the identity tensor, η_{e} the effective viscosity, a_{s} the surface mass balance, a_{b} the mass balance at the ice-bedrock interface, a_{w} the mass balance at the ice-ocean interface, T_{a} the atmospheric temperature, T_{o} the ocean temperature, c_{b} the sliding coefficient, ρ_{i} the ice density, ρ_{w} the water density, g the gravitational acceleration, and m the sliding parameter. The effective viscosity η_{e} is given by Glen's power law as $\frac{1}{2}A^{-1/n}\left|\mathbf{D}(\mathbf{v})\right|_*^{\frac{1}{n}-1}$, with $\left|\mathbf{D}(\mathbf{v})\right|_* = \sqrt{\frac{1}{2}\left(\mathrm{tr}\left((\mathbf{D}(\mathbf{v}))^2\right) + \mathrm{tr}^2\left(\mathbf{D}(\mathbf{v})\right)\right)}$ the effective horizontal strain rate, A the temperature-dependent rheological coefficient, and n the rheological parameter.

In (6.1) and (6.2), the first equation is a depth-integrated conservation of mass equation, with the right-hand side expressing the net mass balance. In (6.1) and (6.2), the second equation is a depth-integrated horizontal mechanical equilibrium equation, expressed as a balance between longitudinal internal stresses, basal friction (in D_{g}), and the gravitational

driving force. These equations, known as the shallow-shelf approximation, follow from an asymptotic thin-film approximation of a nonlinear Stokes problem. In (6.1) and (6.2), the inequality serves as a basis for distinguishing the grounded portion from the floating portion of the domain. These inequalities are deduced from a consideration of vertical equilibrium under a hydrostatic approximation and essentially express Archimedes's law: in the grounded portion, the ice thickness is greater than the thickness at which flotation would occur, whereas in the floating portion, the ice is buoyant in sea water. Hence, the quantity $h + \frac{\rho_w}{\rho_i} b$, called the height above flotation, is positive for grounded ice and negative for floating ice. The height above flotation will serve as the solution quantity of the computational model in our illustration, where interest lies in the retreat of the grounded portion of the AIS.

6.4. Test problem. In order to illustrate the methodology that we propose for constructing confidence sets for excursion sets, we set up a test problem using the f.ETISh model. In this test problem, we simulate the response of the AIS over the next 700 years, starting from its present-day configuration, under a simplified forcing scenario in which the atmospheric and ocean temperatures increase linearly in the first 300 years and then remain constant in the next 400 years. The use of such a simplified forcing scenario is justified by the fact that we do not seek to provide new probabilistic projections and insight into the evolution of the AIS but seek only to demonstrate our proposed methodology. In our test problem, as we set it up using the f.ETISh model, an increase in atmospheric temperature has an impact on the surface mass balance through an increase in precipitation and surface melting, as represented by the dependence of a_s on T_a in (6.1) and (6.2). And, an increase in ocean temperature has an impact on the mass balance underneath the ice shelves through an increase in the strength of the overturning ocean circulation in ice shelf cavities, as represented by the dependence of a_w on T_o in (6.2). We let the forcing scenario be defined as a function of two input parameters. The first input parameter is the change in atmospheric temperature ΔT_a after 300 years, for which we will consider values in the range between 1 and 10 K. To allow the reader to appreciate this range of values, the lower and upper bound are respectively in the range of values for the projected atmospheric temperature increase after 300 years for the strongly mitigated RCP2.6 and the warm RCP8.5 scenario [9]. The second input parameter is the ratio between the change in ocean temperature and the change in atmospheric temperature, for which we will consider values in the range between 0.1 and 0.9; the lower and upper bound account respectively for a slowdown or an amplification of the overturning ocean circulation in ice shelf cavities. Please note that our choice of a wide range of values for the atmospheric and oceanic forcings was also motivated by a desire to trigger significant variability in the retreat of the grounded portion of the AIS and thus obtain a challenging test problem for the proposed methodology. Except for the forcing scenario, the setup of our test problem is similar to the setup of the nominal simulation in [8].

We use a square grid with a length of 5600 km in each direction with a spatial resolution of 16 km and we use a time step of 0.05 year. The computing time of a single simulation on two threads of a SkyLake 2.3 GHz CPU of the Lemaitre 3 cluster (CÉCI clusters, F.R.S-FNRS & Walloon Region, Belgium) is approximately 8 hours.

To illustrate the proposed methodology, we will focus on the grounded portion D_g of the domain at time $\tau = 700$ yr. This portion is determined as the superlevel set of the height

above flotation for the threshold 0, that is,

$$D_{\mathrm{g}} = \left\{ \boldsymbol{x} \in D : y(\boldsymbol{x}) = h(\boldsymbol{x}) + \frac{\rho_{\mathrm{w}}}{\rho_{\mathrm{i}}} b(\boldsymbol{x}) \geq 0 \right\} \text{ for } t = \tau. \tag{6.4}$$

Figure 4 illustrates the evolution of the grounded portion and the grounding line as a function of time for $\Delta T_{\mathrm{a}} = 8.5$ K and $\Delta T_{\mathrm{o}}/\Delta T_{\mathrm{a}} = 0.84$. We observe a limited retreat of the grounding line in the first 200 years, followed by a retreat of the grounding line in the WAIS, especially in the Amundsen sector and in Siple Coast, in the next 200 years. After 700 years, the WAIS has almost completely collapsed as a consequence of a MISI, while vulnerable marine sectors, such as the Wilkes sector, in East Antarctica are undergoing a significant retreat.

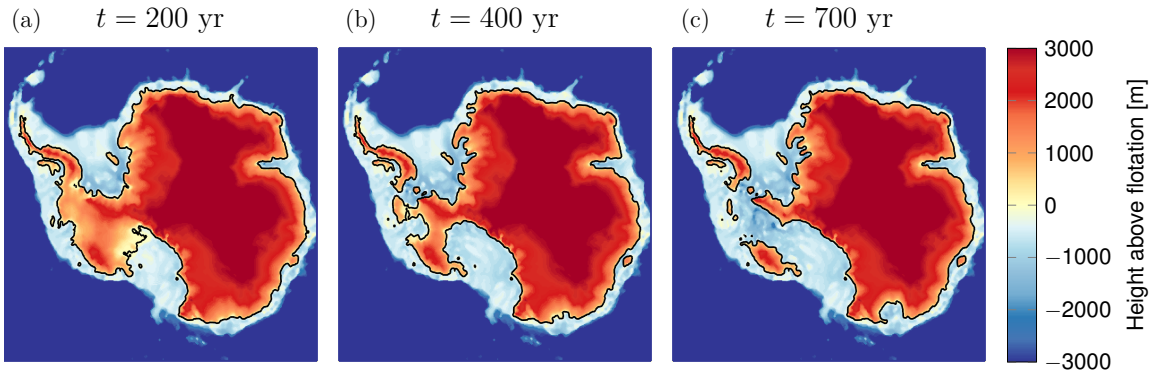

Figure 4. *Illustration of a simulation with $\Delta T_{\mathrm{a}} = 8.5$ K and $\Delta T_{\mathrm{o}}/\Delta T_{\mathrm{a}} = 0.84$. Height above flotation at time (a) $t = 200$ yr, (b) $t = 400$ yr, and (c) $t = 700$ yr. The grounded domain is the set of locations where the height above flotation is larger than 0. The black line is the grounding line.*

6.5. Sources of uncertainty. In our test problem, we consider the two aforementioned input parameters to be uncertain. We represent the change in atmospheric temperature after 300 years with a uniform random variable ξ_1 with values in $[1, 10]$ K. And we represent the ratio between the ocean and atmospheric temperature changes with a uniform random variable ξ_2 with values in $[0.1, 0.9]$. We let ξ_1 and ξ_2 be statistically independent. Similarly to our use of a simplified forcing scenario, our use of such a simplified representation of input uncertainty is justified by the fact that we do not seek to provide new probabilistic projections and insight into the evolution of the AIS but seek only to demonstrate our proposed methodology.

Figure 5 shows the grounded portion for the minimum, mean, and maximum values of the uncertain input parameters. We observe a very limited retreat of the grounding line for the minimum values, an ongoing retreat of the grounding line in the Amundsen and Ronne sectors and in Siple Coast for the mean values, and an almost complete collapse of the WAIS and a retreat of the Wilkes sector for the maximum values.

Upon representing the two uncertain input parameters of the computational model with the aforementioned random variables, the predicted height above flotation becomes the random field $\{Y(\boldsymbol{x}), \boldsymbol{x} \in D\}$. We are interested in its positive excursion set

$$\mathcal{E}_0^+ = \{\boldsymbol{x} \in D : Y(\boldsymbol{x}) \geq 0\}. \tag{6.5}$$

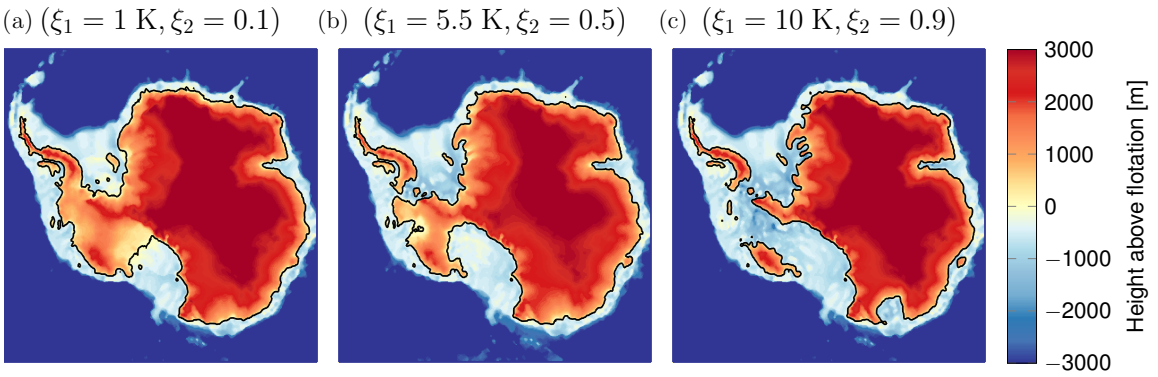

Figure 5. *Height above flotation for the (a) minimum, (b) mean, and (c) maximum values of the uncertain input parameters at time $\tau = 700$ yr. The grounded domain is the set of locations where the height above flotation is larger than 0. The black line is the grounding line.*

For several confidence levels α, we will seek an inner confidence set $C^{\mathrm{in}}_{0^+,\alpha}$ for $\mathcal{E}^+_0$. This inner confidence set $C^{\mathrm{in}}_{0^+,\alpha}$ may be interpreted as the set in which, with a probability of at least α, all locations remain covered with grounded ice. It may also be interpreted as the set to within which, with a probability of at least α, the grounded portion does not retreat with a probability of at least α.

Following the approach of sect. 4, we consider a partitioning of the computational domain and define the excursion sets and confidence sets with reference to this partitioning. Here, the partitioning is taken as a square tessellation of the finite-difference grid points and the representative points are the grid points. The spatial discretization used in the simulations leads to a partitioning into 123201 subsets.

6.6. Membership function. We first generated an ensemble of 500 i.i.d. samples of the uncertain input parameters, from which we deduced the corresponding ensemble of samples of the height above flotation using the computational model. Then, we approximated the pointwise probability density functions of the random field using the kernel density estimation method. Subsequently, we determined the statistical descriptors of the random field from the kernel density estimates. Finally, we evaluated the membership functions defined in (3.15)–(3.17) using the statistical descriptors thus obtained. Figure 6 illustrates these membership functions. We present results for all three membership functions to allow us to comment on the impact of the choice of the membership function on the methodology, for instance, the impact of the membership function on χ. In Fig. 6, both membership functions T_2 and T_3 exhibit a similar behavior, which may be explained by a similar dependence of (3.18) and (3.19) on the coefficient of variation of the random field. The larger difference between T_1 and the two other membership functions may be explained by the non-Gaussianity and bimodality of the random field in regions vulnerable to instabilities as will be shown in sect. 6.7.3.

6.7. Quantile estimation.

6.7.1. Monte Carlo method. As discussed in sect. 5, we may expect the quantile estimation problem to be more computationally challenging than the estimation of the membership

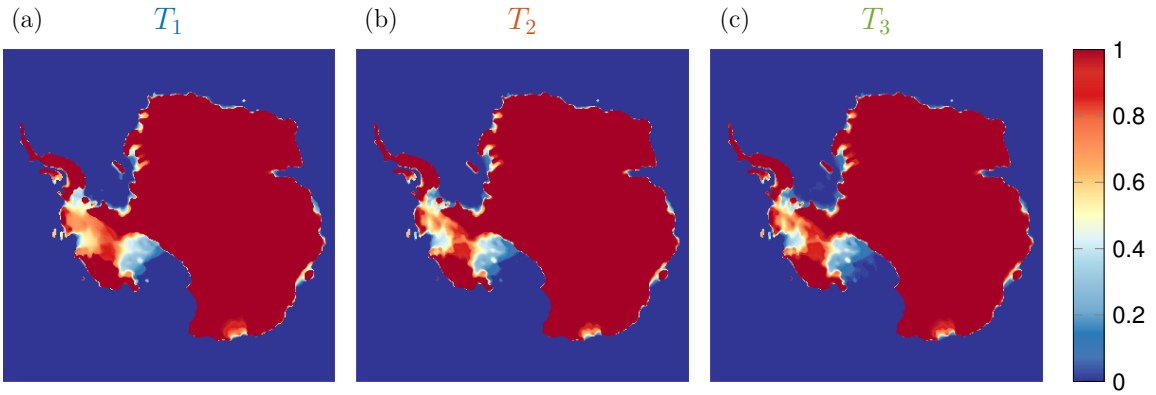

Figure 6. *Membership function: (a) T_1, (b) T_2, and (c) T_3.*

function and we require a higher accuracy of the estimate. Hence, we determined the value of the optimal threshold ρ^* with a larger ensemble of 5000 i.i.d. samples. Owing to the partitioning, χ is a discrete random variable, denoted here explicitly by χ^h, with values in a set with a cardinality of 2815 for T_1, of 2407 for T_2, and of 2440 for T_3. The number of values that χ^h takes is two orders of magnitude smaller than the number of representative points because most representative points are either inside the excursion set or outside the excursion set almost surely and a significant retreat of the grounding line only happens in vulnerable marine sectors. As a consequence of the number of values that χ^h takes being sufficiently large and these values being sufficiently dense, the difference between the distribution function and the mid-distribution function is small, with the magnitude of the discontinuities of the distribution function of the order of 10^{-4} to 10^{-3}. However, both the spatial and the stochastic discretization limit the accuracy in determining confidence sets.

Figure 7(a) shows the sample mid-distribution function for the three membership functions, from which we estimated the corresponding mid-quantiles for the confidence levels 0.5, 0.9, and 0.99. In Figure 7(b), we conducted a numerical convergence analysis to examine the convergence of the Monte Carlo estimates of the mid-quantiles with respect to the number of samples. Figure 7(b) suggests that using 5000 samples is sufficient to ensure a reasonable convergence of the Monte Carlo estimates (see also Table 1). Figure 7(b) also suggests that reasonable convergence of the Monte Carlo estimates is reached for a number of samples larger than 2500.

Table 1 provides the bootstrap mean and two-sigma confidence interval for the Monte Carlo estimates of the optimal threshold ρ^* for the confidence levels 0.5, 0.9, and 0.99. We also determined the area of the resulting confidence sets. Table 1 suggests that using T_1 leads to larger (more optimal) confidence sets than the two other membership functions. For each confidence level α, the inner confidence set for T_1 is well smaller than the corresponding Vorob'ev α-quantile. The use of T_2 and T_3 yields confidence sets of similar size, which is consistent with the similarity that we observed between these membership functions.

6.7.2. Bifidelity method. We will now use the bifidelity method of sect. 5.4, and we will investigate the extent to which it can reduce the computational cost of evaluating the mid-

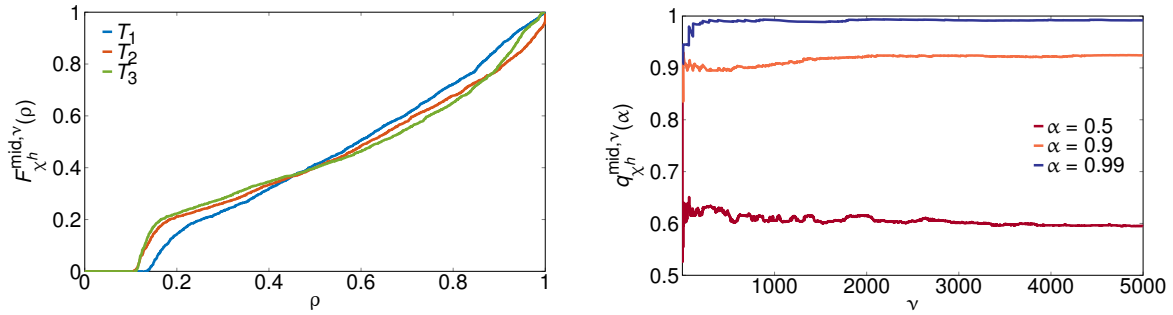

(a) Sample mid-distribution function ($\nu = 5000$).

(b) Convergence analysis of the Monte Carlo estimates as a function of the number of samples ν for T_1.

Figure 7. *Monte Carlo estimates of mid-quantiles.*

Table 1

Boostrap mean and two-sigma confidence interval for the Monte Carlo estimates of the mid-quantiles computed with 10000 *bootstrap replications. The area (millions of km^2) of the resulting confidence sets is reported between parentheses.*

	T_1	T_2	T_3
α	$q^{\text{mid},\nu}_{\chi^h}(\alpha)$	$q^{\text{mid},\nu}_{\chi^h}(\alpha)$	$q^{\text{mid},\nu}_{\chi^h}(\alpha)$
0.5	0.5949 ± 0.0130 (11.027 ± 0.029)	0.6175 ± 0.0158 (10.922 ± 0.033)	0.6432 ± 0.0184 (10.923 ± 0.034)
0.90	0.9240 ± 0.0055 (10.276 ± 0.010)	0.9738 ± 0.0045 (10.199 ± 0.015)	0.9444 ± 0.0035 (10.119 ± 0.014)
0.99	0.9919 ± 0.0025 (10.085 ± 0.014)	1.0000 ± 0.0000 (9.829 ± 0.022)	0.9896 ± 0.0009 (9.829 ± 0.022)

quantiles for the membership function T_1 as compared with the Monte Carlo method used in sect. 6.7.1. We will investigate the use of the two methods for obtaining the surrogate model required for the bifidelity method, namely, the method based on the spectral representation of the random field (sect. 5.3.1) and the method based on the spectral representation of χ^h (sect. 5.3.2). We built polynomial chaos expansions for several choices of the order p using scaled Legendre polynomials whereby we determined the polynomial chaos coordinates from an experimental design made up of the nodes of a fully tensorized scaled Gauss–Legendre quadrature integration rule with $(p+1)^2$ nodes. We implemented the bifidelity method by reusing the ensemble of 5000 i.i.d samples that we had used in the Monte Carlo method in sect. 6.7.1 so as to allow the solution given by the bifidelity method to be compared with the Monte Carlo solution. We used a step size of $\Delta\nu = 50$ and we set $\eta = 0$.

Figure 8 shows a numerical convergence analysis of the mid-quantile estimate as a function of the number of iterations in Algorithm 5.1 using a stochastic expansion of order $p = 5$ either of the random field or of χ^h. In our illustration, we found that Algorithm 5.1 stops when the mid-quantile estimate based on the bifidelity method is equal to the Monte Carlo estimate in Table 1. When $j = 0$, the estimate corresponds to the mid-quantile estimate based on only the surrogate model (see sect. 5.3). We observe that the mid-quantile estimate based on only the surrogate model already provides an accurate estimate of the Monte Carlo mid-quantile. When we apply the bifidelity method, the mid-quantile converges quickly towards

the Monte Carlo mid-quantile, thus suggesting that only a small percentage of evaluations of the computational model is required. We can observe that the bifidelity method converges in fewer iterations for a surrogate model based on a stochastic expansion of χ^h (Fig. 8(b)) than when using one of the random field (Fig. 8(a)).

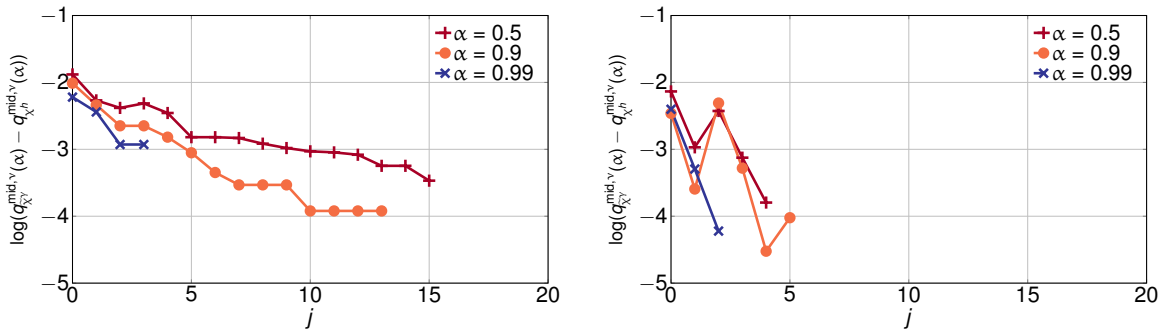

(a) Total CPU time: 6688h for $\alpha = 0.5$, 5888h for $\alpha = 0.9$, and 1888h for $\alpha = 0.99$.

(b) Total CPU time: 2288h for $\alpha = 0.5$, 2688h for $\alpha = 0.9$, and 1488h for $\alpha = 0.99$.

Figure 8. *Convergence analysis of the mid-quantile estimate based on the bifidelity method based on a polynomial chaos expansion either (a) of the random field or (b) of χ^h as a function of the number of iterations in Algorithm 5.1. The absence of data indicates that the mid-quantile estimate based on the bifidelity method is equal to the Monte Carlo estimate. Results are for T_1, order $p = 5$, $\Delta\nu = 50$, and $\nu = 5000$. The equivalent total CPU time, determined from the number of samples of the computational model required to construct the polynomial chaos expansion and to achieve convergence of Algorithm 5.1, is provided as a means of comparison with the Monte Carlo solution (total CPU time of 40000h).*

Figure 9 gives the efficiency of the bifidelity method for a surrogate model based on a polynomial chaos expansion either of the random field (Fig. 9(a)) or of χ^h (Fig. 9(b)) as a function of the order p. We measure the efficiency of the bifidelity method as the number of iterations before exiting Algorithm 5.1, with the maximum number of iterations equal to 100. The number of iterations is high for low orders but drops significantly for higher orders and the 0.99-quantile. Hence, the mid-quantile can be estimated with only a reduced number of samples compared to the Monte Carlo sampling method. In addition, the bifidelity method based on a polynomial chaos expansion of χ achieves a higher efficiency than the bifidelity method based on a polynomial chaos expansion of the random field. Please note that an analysis of the efficiency of the bifidelity method should also take into account the computational cost of constructing the polynomial chaos expansions.

6.7.3. Efficiency of the bifidelity method. We obtained similar convergence and efficiency rates for the other two membership functions. In general, the bifidelity method based on a polynomial chaos expansion of χ^h achieved a higher efficiency than the bifidelity method based on a polynomial chaos expansion of the random field. Also, the bifidelity method based on a polynomial chaos expansion of χ^h showed a higher efficiency for T_1 than T_2 and T_3.

To understand the observations mentioned in the previous paragraphs, we looked at how well the random field and the random variable χ^h lend themselves to being approximated with polynomial chaos expansions. Figure 10(a) shows, as a function of the values taken by the

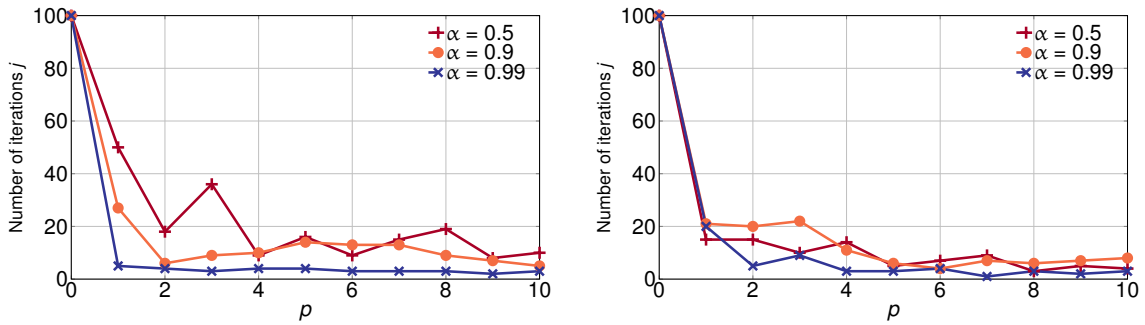

(a) Bifidelity method with polynomial chaos expansion of the random field.

(b) Bifidelity method with polynomial chaos expansion of χ^h.

Figure 9. *Efficiency of the hybrid sampling method: number of iterations before exiting Algorithm 5.1 as a function of the polynomial order p. Results are for T_1.*

uncertain input parameters, the corresponding value taken by the height above flotation at the location $\boldsymbol{x}^*$ in Siple Coast (see Fig. 3). The random variable $Y(\boldsymbol{x}^*)$ has a bimodal distribution with well-separated modes, which suggests the occurence of a MISI in Siple Coast. The higher mode corresponds to small values (low forcing) of the uncertain input parameters and a limited retreat of the grounding line, while the lower mode corresponds to large values (high forcing) of the uncertain input parameters and an important retreat of the grounding line. This suggests that the random field lends itself less well to being approximated with low-order polynomial chaos expansions, especially at locations where a MISI takes place. By contrast, Fig. 10(b)–(c) show, as a function of the values taken by the uncertain input parameters, the corresponding value taken by χ^h for T_1 and T_2, respectively. For small values of the uncertain input parameters, the retreat of the grounding line is limited and the supremum of T in $\left(\mathcal{E}_0^{+h}\right)^{\mathrm{c}}$ is small, while, for large values of the uncertain input parameters, the retreat of the grounding line is important and the supremum of T in $\left(\mathcal{E}_0^{+h}\right)^{\mathrm{c}}$ is large. We can observe that the mapping from the values taken by the uncertain input parameters to the value taken by the random variable χ^h based on either T_1 or T_2 is sufficiently smooth to lend χ^h to better being approximated well with low-order polynomial chaos expansions. In addition, a surrogate model based on a polynomial chaos expansion converges more rapidly towards χ^h for χ^h based on T_1 than on T_2, as may be expected from the mapping from the values taken by the uncertain input parameters to the value taken by random variable χ^h for small values of the uncertain input parameters.

6.8. Confidence sets. In Fig. 11, we represented the confidence sets for the confidence levels 0.5, 0.9, and 0.99. We superimposed these confidence sets to represent risk-assessment maps. We interpret the confidence sets with confidence levels 0.5, 0.9, and 0.99 as the sets for which we have medium, high, and very high confidence the ice sheet will not retreat. Thus, Fig. 11 suggests that, within the context of the test problem as we set it up, there is a medium risk that about half of the WAIS may disappear over the next 700 years and a low risk that the whole WAIS may collapse over the next 700 years. All three membership functions lead to similar interpretations, although the confidence set with confidence level 0.5

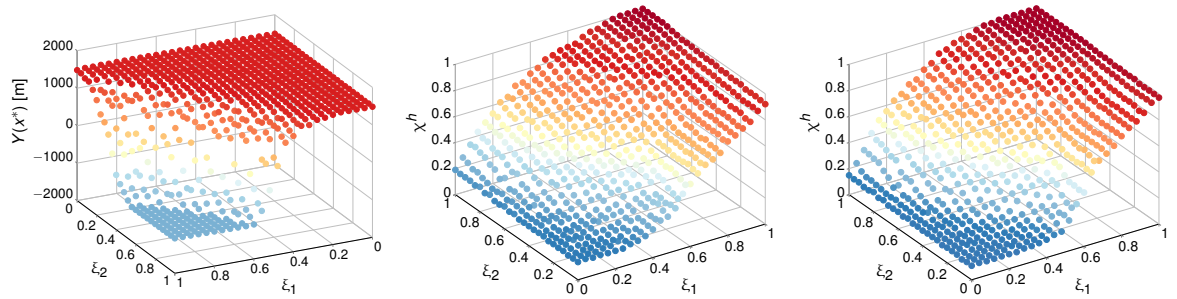

(a) $Y(\boldsymbol{x}^*)$. (b) $\chi^h = \max_{i \in (\mathcal{I}_0^{+h})^c} T_1(\boldsymbol{x}_i^h)$. (c) $\chi^h = \max_{i \in (\mathcal{I}_0^{+h})^c} T_2(\boldsymbol{x}_i^h)$.

Figure 10. *a) Height above flotation at the location $\boldsymbol{x}^*$ in Siple Coast as a function of the values taken by the uncertain input parameters. Value taken by the random variable χ^h as a function of the values taken by the uncertain input parameters for (b) T_1 and (c) T_2.*

for T_2 and T_3 suggests that the WAIS (especially in the Amundsen and Filchner sectors) is more vulnerable than the corresponding confidence set for T_1. Also, the confidence sets for T_3 display the highest vulnerability for the WAIS but the least vulnerability in the Wilkes sector. More generally, such risk-assessment maps may benefit both observational missions and ice-sheet modeling initiatives by indicating critical regions in Antarctica whose evolution has to be tracked and understood in more details.

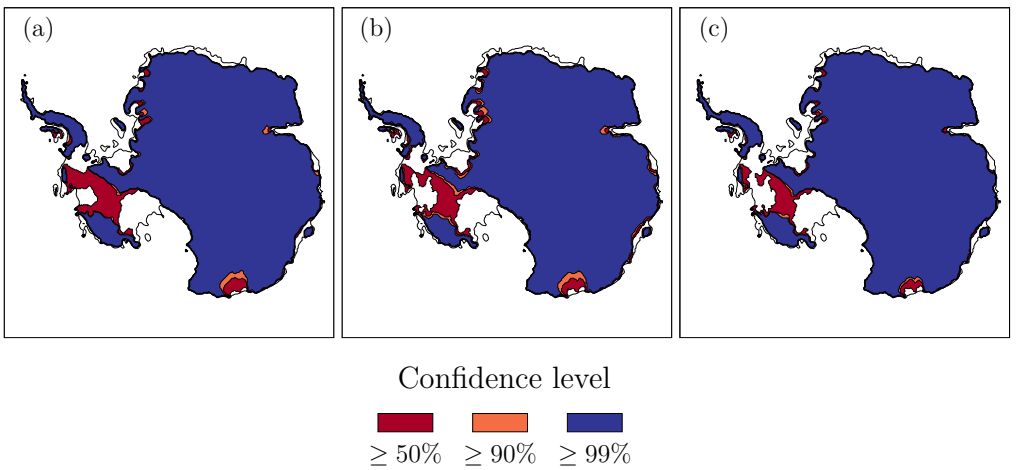

Figure 11. *Risk-assessment maps of the AIS retreat. The blue set, the union of the blue and orange sets, and the union of the blue, orange, and red sets are respectively the confidence set for the confidence levels 0.99, 0.9, and 0.5. Membership function: (a) T_1, (b) T_2, and (c) T_3. The black line is the present-day grounding line. White regions inside the present-day grounding line represent regions where the ice sheet will retreat with high probability (confidence levels less than 0.5).*

6.9. Spatial discretization error. We investigated the impact of the spatial resolution on the results by considering additional spatial resolutions of 32 km, 64 km, and 128 km. Here,

we did not rerun the f.ETISh model for these lower resolutions, but we took the representative points for lower spatial resolutions as subsets of the representative points for higher spatial resolutions. For this reason, the optimal threshold ρ^{*h} for a given confidence level decreases with a decrease of the spatial resolution. Table 2 provides the bootstrap mean and two-sigma confidence interval for the Monte Carlo estimates of the optimal threshold ρ^{*h} (and the corresponding area of the confidence sets) for the confidence levels 0.5, 0.9, and 0.99 for the different spatial resolutions. We observe that the error in the quantile estimation due to the spatial discretization is of the same order of magnitude as the Monte Carlo estimation error for the high resolutions (16 and 32 km). By contrast, the error in the quantile estimation due to the spatial discretization is more significant than the Monte Carlo estimation error for the lowest resolution (16 vs 128 km). Table 2 also suggests that the results for a spatial discretization of 16 km can be considered to have converged with respect to the spatial resolution. Figure 12 shows the corresponding risk-assessment maps for the different spatial resolutions.

Table 2

Boostrap mean and two-sigma confidence interval for the Monte Carlo estimates of the mid-quantiles computed with 10000 *bootstrap replications as a function of spatial resolution (for membership function* T_1*). The area (millions of km*^{2}*) of the resulting confidence sets is reported between parentheses.*

α	0.5	0.9	0.99
	$q_{\chi^h}^{\mathrm{mid},\nu}(\alpha)$	$q_{\chi^h}^{\mathrm{mid},\nu}(\alpha)$	$q_{\chi^h}^{\mathrm{mid},\nu}(\alpha)$
16 km	0.5949 ± 0.0130 (11.027 ± 0.029)	0.9240 ± 0.0055 (10.276 ± 0.010)	0.9919 ± 0.0025 (10.085 ± 0.014)
32 km	0.5937 ± 0.0135 (11.024 ± 0.029)	0.9169 ± 0.0067 (10.275 ± 0.012)	0.9906 ± 0.0030 (10.088 ± 0.012)
64 km	0.5859 ± 0.0165 (11.009 ± 0.04)	0.9148 ± 0.0073 (10.249 ± 0.016)	0.9903 ± 0.0027 (10.055 ± 0.007)
128 km	0.5721 ± 0.0154 (11.037 ± 0.027)	0.9097 ± 0.0047 (10.253 ± 0.020)	0.9793 ± 0.0057 (10.026 ± 0.018)

7. Conclusion. We investigated confidence sets of random excursion sets in the context of stochastic computational models with a high computational cost. We proposed to recast the problem of estimating an optimal confidence set in a parametric family of candidate sets as an equivalent quantile estimation problem of a random variable. We proposed to solve the quantile estimation problem using a surrogate model either of the random field or of the random variable χ, and we introduced a bifidelity method that aims at reducing the approximation error by using the computational model close to the quantile to be estimated. We illustrated this method on a stochastic problem relevant to glaciology and we showed that only a small number of evaluations of the computational model was necessary to achieve an accurate estimate of the quantile. We discussed the impact of the membership function on the efficiency of the bifidelity method, and we concluded that the bifidelity method based on a polynomial chaos expansion of the random variable can be more efficient than the bifidelity method based on a surrogate model of the random field.

The bifidelity method relies on the construction of a surrogate model based on a polynomial chaos expansion, which is especially well suited for low or moderate stochastic dimension. With a methodology-oriented point of view, future work could investigate the stochastic discretization of the quantile estimation problem for computational models with a high stochastic dimension by using, for instance, other methods from reliability engineering such as subset

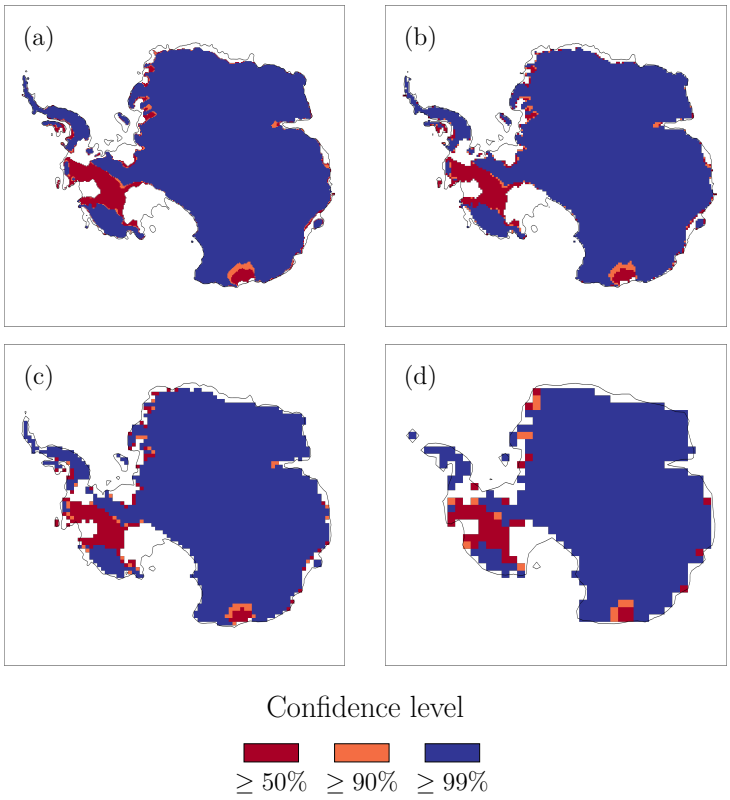

Figure 12. *Impact of the spatial discretization on risk-assessment maps of the AIS retreat (with membership function T_1). Spatial resolutions: (a) 16 km, (b) 32 km, (c) 64 km, and (d) 128 km. The black line is the present-day grounding line for these spatial resolutions.*

simulation or adaptive methods. With an application-oriented point of view, future work could apply the proposed method to provide new probabilistic projections and insight into the evolution of the AIS based on realistic forcings and suitable probabilistic characterizations of uncertain input parameters; see [8] for an example of such an application.

Acknowledgments. Computational resources have been provided by the Consortium des Équipements de Calcul Intensif (CÉCI), funded by the Fonds de la Recherche Scientifique de Belgique (F.R.S-FNRS) under Grant No. 2.5020.11 and by the Walloon Region. The authors also wish to thank two anonymous reviewers for their valuable suggestions that helped improve the content and clarity of the manuscript.

REFERENCES

[1] R. J. Adler, *Some new random field tools for spatial analysis*, Stoch. Environ. Res. Risk Assess., 22 (2008), pp. 809–822.
[2] R. J. Adler and J. E. Taylor, *Random Fields and Geometry*, Springer, New York, NY, 2007.
[3] B. C. Arnold, N. Balakrishnan, and H. N. Nagaraja, *A First Course in Order Statistics*, SIAM, Philadelphia, PA, 1992.

[4] D. Azzimonti, *Contributions to Bayesian set estimation relying on random field priors*, PhD thesis, Universität Bern, Bern, Switzerland, 2016.

[5] D. Azzimonti, J. Bect, C. Chevalier, and D. Ginsbourger, *Quantifying Uncertainties on Excursion Sets Under a Gaussian Random Field Prior*, SIAM/ASA J. Uncertain. Quantif., 4 (2016), pp. 850–874.

[6] M. J. Bayarri, J. O. Berger, E. S. Calder, K. Dalbey, S. Lunagomez, A. K. Patra, E. B. Pitman, E. T. Spiller, and R. L. Wolpert, *Using Statistical and Computer Models to Quantify Volcanic Hazards*, Technometrics, 51 (2009), pp. 402–413.

[7] D. Bolin and F. Lindgren, *Excursion and contour uncertainty regions for latent Gaussian models*, J. R. Stat. Soc. Ser. B Stat. Methodol., 77 (2015), pp. 85–106.

[8] K. Bulthuis, M. Arnst, S. Sun, and F. Pattyn, *Uncertainty quantification of the multi-centennial response of the Antarctic ice sheet to climate change*, Cryosphere, 13 (2019), pp. 1349–1380.

[9] M. Collins, R. Knutti, J. Arblaster, J.-L. Dufresne, T. Fichenet, P. Friedlingstein, X. Gao, W. J. Gutowski, T. Johns, G. Krinner, M. Songwe, C. Tebaldi, A. J. Weaver, and M. Wehner, *Long-term Climate Change: Projections, Ccommitments and Irreversibility*, in Climate Change 2013: The Physical Science Basis. Contribution of Working Group I to the Fifth Assessment Report of the Intergovernmental Panel on Climate Change, T. F. Stocker, D. Qin, G.-K. Plattner, M. Tignor, S. K. Allen, J. Boschung, A. Nauels, Y. Xia, V. Bex, and P. M. Midgley, eds., Cambridge University Press, Cambridge, United Kingdom, 2013, pp. 1029–1136.

[10] G. C. Enss, M. Kohler, A. Krzyżak, and R. Platz, *Nonparametric Quantile Estimation Based on Surrogate Models*, IEEE Trans. Inform. Theory, 62 (2016), pp. 5727–5739.

[11] D. Feldman and H. G. Tucker, *Estimation of non-unique quantiles*, Ann. Math. Statist., 37 (1966), pp. 451–457.

[12] J. French, P. Kokoszka, S. Stoev, and L. Hall, *Quantifying the risk of heat waves using extreme value theory and spatio-temporal functional data*, Comput. Statist. Data Anal., 131 (2019), pp. 176–193.

[13] J. P. French, *Confidence regions for the level curves of spatial data*, Environmetrics, 25 (2014), pp. 498–512.

[14] J. P. French and J. A. Hoeting, *Credible regions for exceedance sets of geostatistical data*, Environmetrics, 27 (2015), pp. 4–14.

[15] J. P. French and S. R. Sain, *Spatio-temporal exceedance locations and confidence regions*, Ann. Appl. Stat., 7 (2013), pp. 1421–1449.

[16] I. R. Goodman and H. T. Nguyen, *Fuzziness and randomness*, in Statistical Modeling Analysis and Management of Fuzzy Data, C. Bertoluzza, M. A. Gil, and D. A. Ralescu, eds., Physica-Verlag, Heidelberg, Germany, 2002, pp. 3–21.

[17] M. Heinkenschloss, B. Kramer, T. Takhtaganov, and K. Willcox, *Conditional-Value-at-Risk Estimation via Reduced-Order Models*, SIAM/ASA J. Uncertain. Quantif., 6 (2018), pp. 1395–1423.

[18] A. Krzyżak, *Recent Results on Nonparametric Quantile Estimation in a Simulation Model*, in Challenges in Computational Statistics and Data Mining, S. Matwin and J. Mielniczuk, eds., Springer International Publishing, Cham, Switzerland, 2016, pp. 225–246.

[19] J. Li and D. Xiu, *Evaluation of failure probability via surrogate models*, J. Comput. Phys., 229 (2010), pp. 8966–8980.

[20] Y. Ma, M. G. Genton, and E. Parzen, *Asymptotic properties of sample quantiles of discrete distributions*, Ann. Inst. Statist. Math., 63 (2011), pp. 227–243.

[21] I. Molchanov, *Theory of Random Sets*, Springer-Verlag, London, UK, 2 ed., 2017.

[22] H. T. Nguyen and E. A. Walker, *A First Course in Fuzzy Logic*, Chapman & Hall/CRC, Boca Raton, FL, 3 ed., 2006.

[23] E. Parzen, *Quantile Probability and Statistical Data Modeling*, Statist. Sci., 19 (2004), pp. 652–662.

[24] F. Pattyn, *Sea-level response to melting of Antarctic ice shelves on multi-centennial timescales with the fast Elementary Thermomechanical Ice Sheet model (f.ETISh v1.0)*, Cryosphere, 11 (2017), pp. 1851–1878.

[25] C. Ritz, T. L. Edwards, G. Durand, A. J. Payne, V. Peyaud, and R. C. A. Hindmarsh, *Potential sea-level rise from Antarctic ice-sheet instability constrained by observations*, Nature, 528 (2015), pp. 115–118.

908 [26] C. Schoof, *Ice sheet grounding line dynamics: Steady states, stability, and hysteresis*, J. Geophys. Res.,
909 112 (2007), p. F03S28.
910 [27] M. Sommerfeld, S. Sain, and A. Schwartzman, *Confidence Regions for Spatial Excursion Sets From*
911 *Repeated Random Field Observations, With an Application to Climate*, J. Amer. Statist. Assoc., 113
912 (2018), pp. 1327–1340.
913 [28] H. Yu, E. Rignot, H. Seroussi, and M. Morlighem, *Retreat of Thwaites Glacier, West Antarctica,*
914 *over the next 100 years using various ice flow models, ice shelf melt scenarios and basal friction laws*,
915 Cryosphere, 12 (2018), pp. 3861–3876.
916 [29] Z. Zou, D. P. Kouri, and W. Aquino, *An Adaptive Sampling Approach for Solving PDEs with Un-*
917 *certain Inputs and Evaluating Risk*, in Proceedings of the 19th AIAA Non-Deterministic Approaches
918 Conference, Gravepine, TX, 2017, American Institute of Aeronautics and Astronautics.